Guidelines for G-quadruplexes: I. In vitro characterization

Yu Luo, Anton Granzhan, Julien Marquevielle, Anne Cucchiarini, Laurent Lacroix, Samir Amrane, Daniela Verga, Jean-Louis Mergny

Guidelines for G-quadruplexes: I. *in vitro* characterization

Yu Luo[1,2], Anton Granzhan[2,3], Julien Marquevielle[4], Anne Cucchiarini[1], Laurent Lacroix[5], Samir Amrane[4], Daniela Verga[2,3*] & Jean-Louis Mergny[1,6*]

Revised Manuscript, submitted to Biochimie on December 19, 2022

1. Laboratoire d'Optique et Biosciences, Ecole Polytechnique, CNRS, Inserm, Institut Polytechnique de Paris, 91128 Palaiseau, France;
2. CNRS UMR9187, INSERM U1196, Université Paris-Saclay, F-91405 Orsay, France;
3. CNRS UMR9187, INSERM U1196, Institut Curie, PSL Research University, F-91405 Orsay, France;
4. Université de Bordeaux, ARNA Laboratory, INSERM U1212, CNRS UMR 5320, IECB, 33076 Bordeaux, France;
5. Institut de Biologie de l'Ecole Normale Supérieure (IBENS), Ecole Normale Supérieure, CNRS, INSERM, Université PSL, Paris, France;
6. Institute of Biophysics of the Czech Academy of Sciences, Brno, Czech Republic.

* Authors to whom correspondence may be addressed: **daniela.verga@curie.fr**; **jean-louis.mergny@inserm.fr**

Abstract

Besides the well-known DNA double-helix, non-canonical nucleic acid structures regulate crucial biological activities. Among these oddities, guanine-rich DNA sequences can form unusual four-stranded secondary structures called G-quadruplexes (G4s). G4-prone sequences have been found in the genomes of most species, and G4s play important roles in essential processes such as transcription, replication, genome integrity and epigenetic regulation. Here, we present a short overview about G-quadruplexes followed by a detailed description of the biophysical and biochemical methods used to characterize G4s in *vitro*. The principles, experimental details and possible shortcomings of each method are discussed to provide a comprehensive view of the techniques used to study these structures. We aim to provide a set of guidelines for standardizing research on G-quadruplexes; these guidelines are not meant to be a dogmatic set of rules, but should rather provide useful information on the methods currently used to study these fascinating motifs.

Keywords

G-quadruplexes; Nucleic acids; Structure determination; Spectroscopy; Quadruplex ligand

1. Introduction

Nucleic acids are biological macromolecules found in all life forms, made up of nucleotides which encode genetic information. The vast majority of DNA probably adopts a B-type DNA (B-DNA) double-helical structure under physiological conditions. In 1953, J. Watson and F. Crick determined the helical structure of double-stranded (ds) DNA using X-ray diffraction data collected by R. Franklin [1]. The structure consisted of two complementary single-strands (ss) held together by nucleobase stacking and the formation of inter-strand hydrogen (H-) bonds connecting nucleobases. These H-bonds are now often referred to as 'Watson–Crick hydrogen bonds' [2, 3]. Asides from the classic duplex, DNA and RNA can also adopt alternative secondary structures involving two or more strands [4, 5]. Z-DNA, for example, is a left-handed double-helix where the sugar-phosphate backbone is arranged in a *zig-zag* shape giving the structure its Z-DNA name. Z-DNA has been identified to be implicated in gene activation, chromatin remodeling and large-scale genomic deletions in mammalian cells [6], and was recently reported to be a major component of extracellular DNA in bacterial biofilms [7]. Nucleic acids can form three-stranded structures or triplexes (based on base triplets such as CG•CH+ and CG•G, *etc*.) [8, 9] and four-stranded structures such as *intercalated* DNA (i-DNA) or G-quadruplexes (G4s), as well as other oddities [10, 11] such as penta-stranded structures [12].

In 1989, Williamson *et al.* reported that telomeric G-rich sequences may adopt a G-quadruplex fold, as shown by anomalous electrophoretic mobility in polyacrylamide gels [13]. Since then, multiple G4-forming sequences have been characterized and G4 structures have been shown to be involved in important biological processes, such as genome stability, gene transcription and expression [14], specific chromatin remodeling and replication [15, 16]. G4s in RNAs have been related to pre-mRNA processing (splicing and polyadenylation), mRNA turnover, RNA metabolism [17], mRNA localization, and translation [18].

2. Structures of G-quadruplexes (G4)

G-quadruplexes constitute a family of secondary structures formed by Guanine (G)-rich nucleic acid sequences. Four Guanine bases are connected by Hoogsteen hydrogen bonds to form a *G-tetrad*, or a *G-quartet*, the basic unit to form a G4, which was first proposed by Gellert *et al*. in 1962 [19]. Metal ions play a significant role in the stabilization and stacking of G-tetrads, and potassium and sodium are the most common cations used to stabilize these structures [20]. The π-stacking of two or more G-tetrads generates a quadruplex structure.

G-quadruplexes are highly polymorphic. As guanine nucleotides may adopt *anti* and *syn* conformations, the arrangement and combination of *anti* and *syn* guanines results in different types of G-tetrads with varied grooves and stacking features. G4s can be classified into parallel (**Figure 1a**), hybrid (**Figure 1b**), and anti-parallel (**Figure 1c**) structures according to the orientation of the strands [21]. According to loop types, anti-parallel structures can be further subdivided into chair and basket conformation. Depending on the number of strands involved in the G4 assembly, G4s can be categorized into mono- (intramolecular), bi-, tri- and tetra-molecular structures, while higher-order structures may also be obtained [22].

RNA G4s tend to be more stable than the DNA G4 of the corresponding sequence (for example, when comparing d(TGGGT) with r(UGGGGU) [23, 24]. The 2′-hydroxyl group imposes additional steric constraints on the G4 topology, where it prevents – or strongly disfavors – the base from being oriented in the *syn*-conformation and imposes constraints on sugar pucker, allowing only the C3′-*endo* form. As a result, RNA G4 structures are nearly always restricted to the parallel topology, in which all four strands go in the same direction [25] while DNA G4s can adopt parallel, anti-parallel, and hybrid structures.

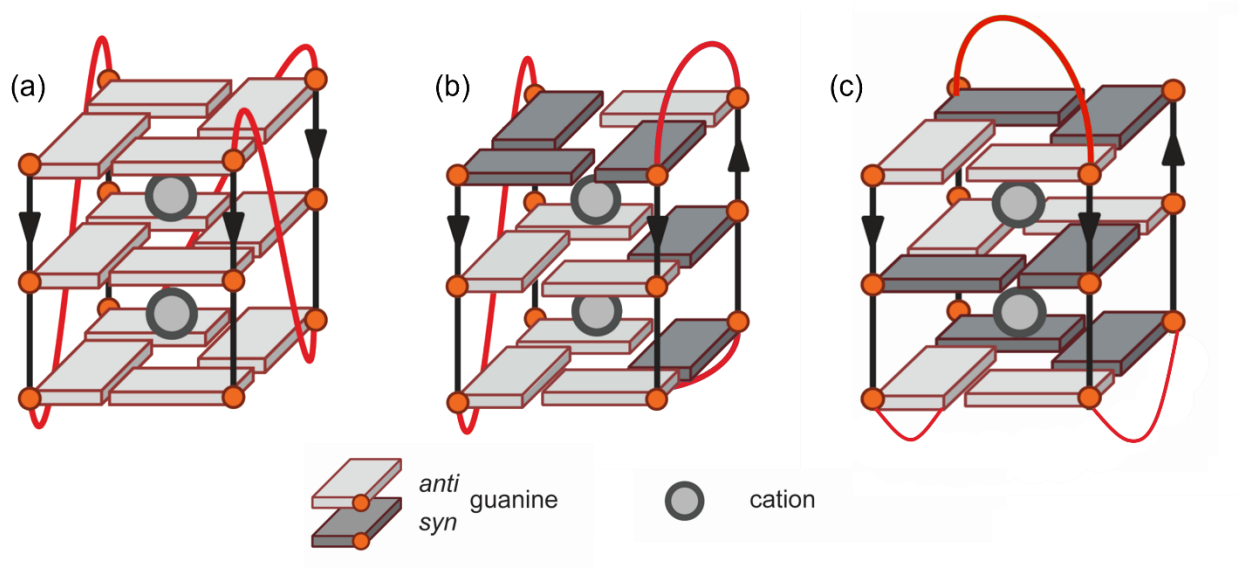

*Figure 1 Schematics of (**a**) parallel G4; (**b**) hybrid G4 and (**c**) anti-parallel G4.*

Topologies and stabilities of G4s are affected by several factors:

i) *Temperature*: Like most nucleic acid secondary structures (with a possible exception for a purine triplex [26]), G4 formation is enthalpy-driven, and quadruplexes tend to unfold at high temperature. Thermal stability is highly sequence-dependent: while some super-stable G4s may resist boiling, other quadruplexes are barely stable at physiological temperature. In general, it is possible to stabilize G4 structures with small-molecule ligands [27, 28].

ii) *Ionic environment*: Metal cations can stabilize G4s by laying between two G-tetrads or by staying in the plane of a G-tetrad. The general trend of G4 stabilized by monovalent and divalent cations is $Sr^{2+} > Ba^{2+} > K^{+} > Ca^{2+} > Na^{+}$, NH_4^{+}, $Rb^{+} > Mg^{2+} > Li^{+} \geq Cs^{+}$ [29]. The type and concentration of metal ions also have an effect on G4 topology [30].

iii) *Molecular environment*: Crowding conditions have been reported to preferentially stabilize G4 structures. Polyethylene glycol (PEG) is a widely used crowding agent, which may convert G4 topologies from anti-parallel to parallel in sodium buffers [31]. However, other crowding agents may have different effects – PEG is not a true crowding agent, and stabilization may not only be related to crowding effects as observed for example for i-DNA [32]. Regarding G-quadruplexes, PEG binds G4 based on conformational selection leading to the observed conformational

transition [33].

iv) *Loop length*: In potassium buffers, the total loop length is inversely correlated to G4 thermal stability: each added base leads to a 2 °C drop in T_m [34], and only a few G4s with a loop of more than 7 nt have been reported (*e.g.*, [35]). Loop length also effects G4 topology. Generally, very short linkers (1 or, to a lesser extent, 2-nt long loops) impose chain reversal loops, which impose a parallel topology. On the other hand, longer linkers are compatible with all types of loops and non-parallel topologies may be observed. A loop of moderate length (2-3 nt) enables both parallel and anti-parallel conformations to form [36]. Recently, we illustrated that loop permutation also influences G4 stability and topology [37]. Additionally, loop length has been associated with G4 molecularity, two short loops (1–2 nt) have been shown to favor intermolecular complexes in potassium [34].

v) *Flanking nucleotides*: The core G4 motif may be flanked by one or more nucleotides at both extremities. The addition of flanking nucleotides favors a parallel topology, and flanking nucleotides at the 5' end exert a greater influence on topology than those at the 3' end [38]. The presence of nucleotides at the 5' end prevents a strong *syn*-specific hydrogen bond for a 5'-terminal guanine which is frequently observed in non-parallel conformations [38].

3. Characterization of G-quadruplexes *in vitro*

With the development of bioinformatics and high-throughput sequencing, putative G-quadruplex sequences (PQS) have been identified in numerous genomic loci, including telomeric regions, ribosomal DNA, the immunoglobulin heavy chain region, as well as transcriptional regulatory regions of a number of genes, especially oncogenes [14]. PQS are also present in mitochondrial DNAs [39] and chloroplast DNAs [40]. However, identifying a guanine-rich sequence does not necessarily mean it can (or will) form a G4 structure *in vitro*. Hereafter, we introduce different biophysical methods which have been included in our ‘G4 characterization toolbox’. Our previous experience has demonstrated that one could reach contradictory conclusions depending on the technique used [41], and some possible caveats will be discussed below. We thus recommend to use a combination of these approaches to validate G4 formation by a given sequence.

There are a few trivial considerations to be discussed regarding the different experimental approaches. First, we have systematically chosen to express DNA concentration as the concentration in oligonucleotide strands rather than in nucleotides, as the secondary structures are constructed by strands, not by individual nucleotides. Of note, this definition may be impractical in some cases:

i) For polynucleotides, whose exact length is not precisely known; in the case where polynucleotides need to be added to the panel of studied nucleic acids, we recommend expressing their concentration in nucleotides (or phosphates) and adjust to the average nucleotide concentration in oligonucleotide samples;

ii) For multimeric structures, *e.g.*, long oligonucleotides capable of forming two or more G4

structures on the same strand;

iii) For intermolecular structures involving two or more strands.

In the two latter cases the concentration should be rather expressed in structural units (*e.g.*, 'quadruplexes') rather than in oligonucleotide strands. In any case, whatever reference is chosen, the concentration can be readily converted from one reference state to another by, in the case of defined oligonucleotides, the known length. That is, for example, the concentration of a 1 µM solution of a 24-nt oligo would simply be 24 µM with respect to nt.

Of note, the precise determination of oligonucleotide concentration may not be as trivial as it seems, as its theoretical extinction coefficient (provided by the manufacturer, or calculated using nearest-neighbor approximation methods) may be not very accurate for purine-skewed sequences. In addition, the sample needs to be unfolded for this extinction coefficient to be applicable. Denaturation may be facilitated by preincubation at high temperature (95 °C) for 3–10 minutes (depending on the length of the strands) in the absence of salts. On the other hand, the acquisition of absorbance or CD spectra of the folded form requires that the sample is properly folded. Pre-annealing of DNA or RNA in the buffer of interest, followed by either slow or rapid cooling should allow the oligonucleotides to adopt thermodynamically or kinetically-favored structures, respectively.

3.1 UV–visible absorbance spectroscopy

UV–visible absorbance is a simple and often overlooked experimental technique to analyze nucleic acid conformations. The spectroscopic properties of DNA/RNA depend on their nucleotide content, on the properties of the solvent, and the structure adopted. Absorbance in the far UV region (around 190 nm) arises from the sugar-phosphate backbone, while longer-wavelength absorbance (200 to 300 nm) is entirely attributable to electronic transitions of purine and pyrimidine bases [42]. In the double-stranded helix, base pair stacking leads to a decrease in UV absorbance at 260 nm. This phenomenon is called hypochromicity, whereas hyperchromicity refers to the opposite phenomenon in which absorbance is increased.

The characteristic UV absorption features of quadruplexes are different from those of the double helix. Guanosine has two π–π^* transitions at 245 nm and 275 nm [43], while the formation and dissociation of intramolecular G-tetrads can be precisely monitored by absorbance changes at 295 nm [44]. Based on the characteristic transition around 295 nm, there are three biophysical ways to characterize G4 structures *in vitro* discussed below.

3.1.1 Isothermal differential spectrum (IDS)

As discussed above, different cations can stabilize G4 structures; they are actually required for proper G4 folding: in the absence of these cations (*i.e.*, in pure water or in a buffer containing only non-stabilizing cations such as Li^+) most G-rich sequences remain unfolded, whereas the addition of a suitable cation

(Na^+, K^+, etc.) promotes folding. One may then be able to record the absorbance of the folded and unfolded species at the same temperature (**Figure 2a**). The first absorbance spectrum is therefore recorded under conditions that do not promote G4 formation (*i.e.*, buffer containing no favorable ions like Na^+ or K^+); alkali metal salt (NaCl or KCl) is then added, and a second spectrum is recorded after a suitable incubation time (generally short for intramolecular structures; 5 min should be sufficient to allow at least partial folding); a proper correction for dilution must be applied for the second spectrum, as the volume of the added salt is not negligible (typically, 5 to 10%). The difference between these two spectra is called an isothermal difference spectrum or IDS:

$$\text{IDS} = \text{Spectrum in the absence of cation} - \text{Spectrum in the presence of cation}$$

The IDS of a G4-forming sample has a specific shape, with a negative peak at 295 nm (**Figure 2c**). For most sequences studied in the lab, we chose to perform IDS at 25 °C (or room temperature) but nothing prevents the experiment to be performed at physiological temperature or, for unstable structures, at 4 °C. We use potassium to induce G4-formation and set the final K^+ concentration to 100 mM; the majority of G4 structures are stabilized under these conditions (some quadruplexes actually require much lower potassium concentration to fold!).

3.1.2 Thermal differential spectrum (TDS) [45]

TDS corresponds to the difference between the absorbance spectra at high (typically, 95 °C) and low temperatures (typically, 25 °C) in a buffer favorable for G4 formation (**Figure 2b**). Usually, the samples are kept in a lithium cacodylate buffer supplemented with 100 mM K^+.

$$\text{TDS} = \text{Spectrum at 95 °C} - \text{Spectrum at 25 °C}$$

Since secondary structures unfold at high temperature, the spectrum recorded at 95 °C should correspond to the unfolded species, while the lower temperature spectrum may correspond to the folded species. The negative peak at 295 nm (**Figure 2d**) suggests G4 unfolding at high temperature.

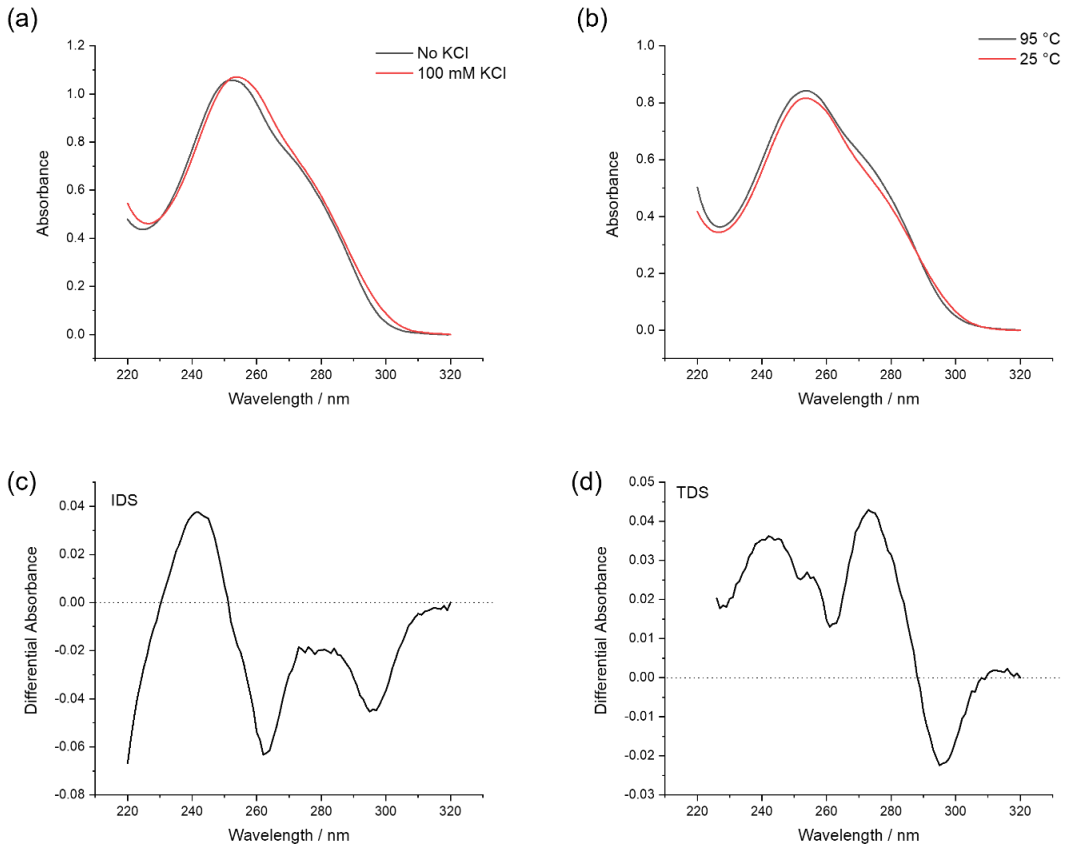

*Figure 2 UV spectra of pre-folded 3 μM d[GTGGTGGCG$_4$TG$_4$ACG$_6$]. All spectra were recorded on a Cary 300 spectrophotometer (Agilent Technologies) in 1-cm pathlength quartz cuvettes (scan range: 320–220 nm; scan rate: 600 nm/min; automatic baseline correction). (**a**) UV absorbance in the absence (black line) or in the presence (red line) of 100 mM KCl in 10 mM lithium cacodylate (LiCaco) buffer, pH 7.2. Both spectra were recorded at 25 °C; (**b**) UV absorbance at high (95 °C, black line) or low (25 °C, red line) temperatures. Both spectra were recorded in 100 mM KCl, 10 mM LiCaCo buffer, pH 7.2; (**c**) Isothermal differential absorbance spectra (IDS) of the two curves shown in panel (a); (**d**) Thermal differential absorbance spectra (TDS) of the two curves shown in panel (b).*

3.1.3 General considerations on TDS and IDS

Both IDS and TDS are based on the same principle:

$$\text{TDS or IDS} = \text{Spectrum } \textit{unfolded} - \text{Spectrum } \textit{folded}$$

TDS (and to a lesser extent IDS) are now widely used methods to characterize G4 structures *in vitro*. IDS and TDS share some properties, but are not identical: while both TDS and IDS of a G4-forming sequence exhibit a negative peak around 295 nm, significant differences will be observed at shorter wavelengths. This results from an often-overlooked consideration: the unfolded species in both differential spectra are actually different, as they correspond to high temperature or low salt conditions. We also know that the

absorbance properties of the folded and unfolded species depend on temperature, and this property will "pollute" the TDS. The following comments regarding these two differential spectra should be considered:

i) The absence of a negative peak around 295 nm is often a strong argument against G4 formation [45] (exceptions will be commented in the next paragraph). However, the opposite is not true: a hypochromism at 295 nm is not specific for G4 formation as other structures exhibit the same trend. Still, this negative peak may become a good argument for G4 formation if its presence is K^+-dependent. We present the TDS of several DNA secondary structures detailed in Table 1 [45]. Besides G4 structures, other high-ordered structures (*i.e.*, i-motif and pyrimidine triplexes) and some non-B duplexes (such as Z-DNA and parallel Hoogsteen duplexes), also give negative peaks at 295 nm. Thus, G4 formation cannot be validated based on this feature only. However, the overall *shape* – not only the region around 295 nm – of the TDS seems to be specific for G4, allowing to discriminate between all these structures based on IDS or TDS only.

Table 1 Significant TDS peaks of secondary structures [45]

Secondary structures	Hydrogen bonds	Stands orientation	Significant TDS peaks*
B-DNA AT duplex	Watson-Crick	anti-parallel	260 nm (+), 280 nm (−)
B-DNA GC duplex	Watson-Crick	anti-parallel	238 nm (+), 278nm (+)
Z-DNA	Watson-Crick	anti-parallel	240 nm (+), 275 nm (+), 295 nm (−)
Parallel AT duplex	Reverse Watson-Crick	parallel	260 nm (+), 280 nm (−)
Pyrimidine triplexes	Watson-Crick	hybrid (2+1)	Variable positive peak in 240 to 275 nm; 295 nm (−)
G4	Hoogsteen	variable	240 nm (+), 275 nm (+), 295 nm (−)
i-motif	C•CH+	two duplexes anti-parallel to each other	240 nm (+), 295 nm (−)

** (+) and (–) indicate local maxima and minima of the TDS, respectively.*

ii) While the absence of a negative TDS or IDS signal at 295 nm generally indicates that the sample is *not* folding into a G4 structure, there are several exceptions to this rule. As both TDS and IDS correspond to the difference between unfolded and folded states, one has to check that the denaturing conditions (no salt or high temperature) are sufficient to unfold the G4 structure. Indeed, some very stable G4s may fold even in the presence of trace amounts of metal ions, and/or resist boiling (*e.g.*, the T_m of 19wt in 100 mM KCl is higher than 90 °C [46]). As a result, the "denatured" state remains folded, and the TDS/IDS are affected. This artefact may be identified by recording the CD spectra of the "unfolded" state: if the signal is intense under these conditions, the structure cannot be considered unfolded.

iii) One should select a buffer that does not absorb light in the far-UV region (Tris is often unsatisfactory at wavelengths below 240 nm). Cacodylate (pK_a = 6.14) and acetate (pK_a = 4.62) are appropriate choices when working at neutral or slightly acidic pH. They offer the additional benefit of having a nearly temperature-independent pK_a [45], meaning that the pH of the solution will not change much with temperature: while a moderate pH change should not be a major issue for G4 structures, it will strongly affect the stability of other conformations such as pyrimidine triplexes or i-motif. We generally use 10 mM lithium cacodylate (LiCaco) for near-neutral conditions, prepared from cacodylic acid and lithium hydroxide. In addition, chloride salts (UV cutoff: 205 nm) should be avoided or replaced with perchlorate (ClO_4^-) or fluoride (F^-; not compatible with Li^+) counterparts if information in the short-wavelength region (190–210 nm) is critical.

3.1.4 UV-melting

A UV-melting experiment is commonly used to determine the stability of a complex. When a sample is heated, its absorbance properties change, indicating a conformational change in the molecule(s) in solution [47]. Heating denatures nucleic acid secondary structures and affects absorbance properties, which allows one to follow the denaturation of a secondary structure. The melting temperature (T_m) of secondary structures refers to the temperature at which 50% of the oligonucleotide is unfolded. The absorbance at 295 nm allows one to follow folding and unfolding of G-quadruplexes. We previously published detailed experimental procedures and data analysis [47, 48]. We suggest performing UV-melting with ~3 μM (presumably) pre-folded samples (longer oligonucleotides will be studied at a lower strand concentration, in order to keep nucleotide concentration and absorbance in an acceptable range). As shown in **Figure 3a**, the precise absorbance measurement range of typical UV-vis spectrometers is between 0.1 and 2.0, while a too low or a too high concentration may lead the absorption out of this range. A typical temperature range can be 4 °C to 95 °C, but may be shrunk to a smaller interval if one has indications on the stability of the structure: there is no need to go below room temperature if the structure is expected to be very stable. The T_m of a G4 structure may sometimes be too high to be measured (**Figure 3b)**, when there is no plateau at high temperature where the structure has melted completely. We summarize the additional points that should be taken into consideration in the following:

i) A negative transition at 295 nm *per se* is not indicative of G4 unfolding: other structures (pyrimidine triplexes, i-motif) will also lead to a decrease in absorbance upon melting at this wavelength. Thus, T_m determination will give an indication on the thermal stability of the structure but not on its nature.

ii) A strong indication of a G4 structure is the dependence of its T_m on the nature of the cation. Performing melting experiments in KCl, NaCl, and LiCl may give precious clues: for a typical quadruplex, $T_m(K^+) \geq T_m(Na^+) > T_m(Li^+)$. Quantitative differences depend on the nature of the quadruplex: for example, for some G4 RNAs, the T_m in Na^+ may be very close to the T_m in Li^+, but the stability is typically much higher in K^+.

iii) For some extremely stable G4s (or G4 structures stabilized by ligands), performing UV-melting in 100 mM K^+ may be inadequate to observe the melting transition or to determine the T_m value. Lowering potassium concentration to 1, 5 or 10 mM may help, but total monovalent ion concentration can be kept stable by mixing Li^+ and K^+.

iv) The solutions should be degassed prior melting to avoid the formation of air bubbles upon heating. If the sample is not heat-sensitive, this can be easily achieved by briefly heating the solution, then gently remove the bubbles formed (longer heating would lead to evaporation). Otherwise, degassing in a vacuum chamber or sonication (during at least 5 min) are convenient alternatives.

v) Condensation of water on cuvette windows at temperatures below the dew point (≤ 20 °C) can be minimized by blowing a stream of dry air or nitrogen gas on the outer cuvette surfaces [48].

vi) T_m depends on strand concentration for intermolecular structures, but is concentration-independent for intramolecular structures. The analysis of T_m as a function of strand concentration may therefore provide additional information on the nature of the secondary structure, as long as a wide-enough range of concentrations is used (a 5 to 10-fold change is recommended) and that the transition is clear enough to allow a precise T_m determination. One may use quartz cuvettes different light paths to avoid problems with high absorbance.

vii) A *hysteresis* phenomenon may occur, meaning that the heating and cooling profiles may not be superimposable. This means that the denaturation / renaturation experiment is not at thermodynamic equilibrium and that thermodynamic parameters cannot be directly extracted from these curves. The kinetics of intramolecular G4 formation tend to be fast enough to avoid this phenomenon, unless very fast temperature gradients are used, while inter-molecular quadruplexes often lead to a strong hysteresis, especially in the case of tetramolecular G4s [23]. This feature is not discussed here in details as it should not affect the conclusion regarding G4 formation or not.

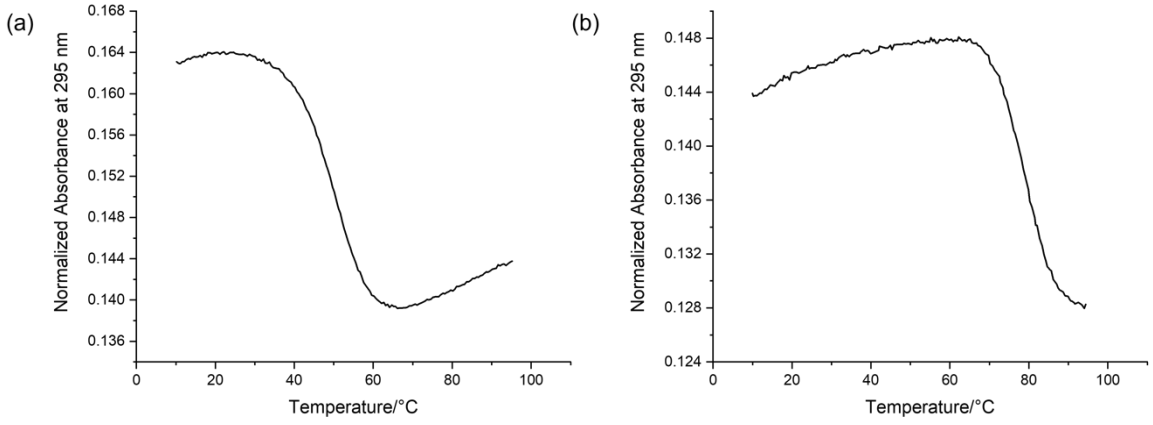

*Figure 3 UV-melting profiles of folded 3 μM (**a**) d[$AG_3AG_3CGCTG_3AGGAG_3$] and (**b**) d[$CG_3CG_3T_3CG_3CG_3T$] in 100 mM KCl, 10 mM LiCaCo buffer, pH 7.2. All spectra were recorded on a*

Cary 300 spectrophotometer (Agilent Technologies) with 10 mm pathlength quartz cuvettes. Heating runs were performed between 10 °C and 95 °C, the temperature was increased by 0.2 °C/min, data interval was set as 0.5 °C and absorbance was recorded at 295 nm.

Interestingly, monitoring of absorbance at four wavelengths (245, 260 and 275 nm in addition to G4-specific 295 nm) during UV-melting experiments allows to identify the topology of a G4 structure, since the corresponding melting profiles are topology-specific [49]. Proper T_m determination may be performed provided that accurate baselines may be drawn below and above T_m. This is the case for panel (a) in **Figure 3**, but less so for panel (b): accurate T_m and van't Hoff enthalpies will be less accurately determined in the latter case.

3.2 Circular dichroism (CD) spectroscopy

Circular dichroism is largely empirically used in the study of the secondary structures of biomacromolecules, mostly proteins and nucleic acids. CD is relatively sensitive, allowing to study nucleic acids at strand concentration in the micromolar range, *i.e.*, lower than the one required for NMR studies. The CD spectra are particularly used in monitoring changes in a secondary structure during titration, binding, or thermal denaturation experiments [50]. In brief, any change in chirality can be followed by circular dichroism.

CD is especially useful to study G-quadruplexes, as this technique not only provides information on the nature of the structure (G4 or not), but also on the topology of the quadruplex, provided sufficient precautions are taken to exclude alternative structures that would show peaks in the same wavelength range (see below). In addition, provided a rigorous quantitative analysis is performed, it may also provide information on the number of quartets formed (see below). This sensitivity stems from the sequential arrangement of quartets, which depends on the topology. To understand stacking between two quartets, one can think of two coins stacked together (**Figure 4**): they can be head-to-tail (H-to-T), head-to-head (H-to-H), or tail-to-tail (T-to-T) (**Figure 4b**). Every stacking interaction, when more than two quartets are involved, may also be H-to-T, or H-to-H, or T-to-T. The following convention may be used: the "head" side G-tetrad corresponds to the side in which the hydrogen bonds run clockwise from donor to acceptor, while seen from the "tail" side they are counter-clockwise [51]. Generally, all guanosines in parallel G4s adopt an *anti* conformation and homopolar H-to-T stacking, with a positive ellipticity at 260 nm and a negative one at 240 nm (**Figure 4c**). In hybrid G4s involving both H-to-T and H-to-H arrangements, the characterized CD pattern also exhibits negative and positive bands at around 245 and 260 nm, respectively, with an additional predominant positive band at around 295 nm (**Figure 4d**). This extra positive band probably arises from the stacking of G-tetrads with alternating polarities, as the combination of *anti* and *syn* glycosidic bond angles (GBA) alternate the polarity of G-tetrads [52]. G-tetrads adopt H-to-H and T-to-T stacking in anti-parallel quadruplexes, leading to a CD pattern far different from the one of parallel G4s, with a negative band at 260 nm and two positive bands at 240 and 295 nm (**Figure 4e**). Note that the CD signal above 220 nm exclusively results from the bases, not from the backbone. For example, the self-arrangement of guanosine nucleotides into a "G4-like" structure generates a strong CD signal, resulting from the stacking of multiple quartets which are not covalently

linked through a sugar-phosphate backbone [53]. It should be noted that the CD spectra are less solid to evidence G4 forming (especially for parallel G4s), as several other structures also show CD signal in 260-270 nm.

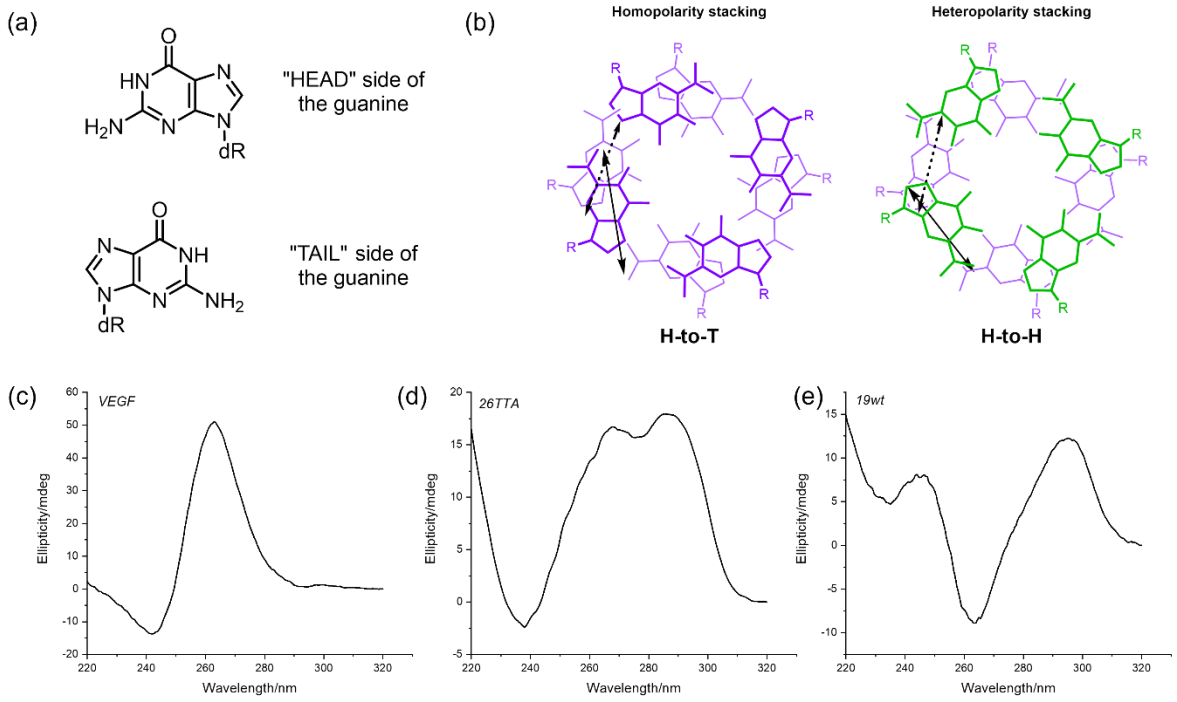

*Figure 4 (**a**) Schematic depictions of the 'head' and 'tail' sides of the guanine. (**b**) Top view of the homopolar (head-to-tail) and heteropolar (head-to-head) and stacking of two G-quartets. The "head" and the "tail" sides of G-tetrads are represented in violet and green, respectively. The double-head arrows represent the transition moments corresponding to the absorption at 250 nm. CD spectra of 5 μM pre-folded (**c**) VEGF (d[$CG_4CG_3CCTTG_3CG_4T$], PDB: 2M27, parallel G4) and (**d**) wtTel26 (d[$(TTAGGG)_4TT$], PDB: 2JPZ, hybrid G4) in 100 mM KCl, 10 mM LiCaCo buffer, pH = 7.2; (**e**) 19wt (d[$G_5(AG_4TAC)_2AG_4$], PDB: 6FTU, anti-parallel G4) in 100 mM NaCl, 10 mM LiCaCo buffer, pH = 7.2. CD spectra were recorded on a J-1500 spectropolarimeter (JASCO) at 25 °C, using a scan range of 320–220 nm, a scan rate of 100 nm/min and averaging four accumulations.*

Raw CD spectra are expressed in ellipticity θ [mdeg] versus wavelength. A useful operation is to properly normalize CD for pathlength and concentration, which can be expressed as molar circular dichroism Δε [cm^{-1} M^{-1}] or as molar ellipticity. One can use the formula: $\Delta\varepsilon = \theta / (32980 \times c \times l)$ to perform this conversion, where c is the oligonucleotide concentration (in M) and l is the optical length (in cm). Proper normalized amplitudes are essential for quantifying G-quartets stacking. For parallel G4s, the CD peak around 265 nm amplitude correlates with the number of G-tetrads in intramolecular quadruplexes [54]. In addition, as the monomer, dimer and interlocked G4 structures have different numbers of stacking interactions (monomer < dimer < interlocked), the CD amplitudes at 265 nm may provide clues on molecularity, as higher amplitudes may be found for higher-ordered structures [55].

A variety of structural factors (loop types [56], sugar-phosphate backbone, strand orientation, and chemical modifications of guanines) may affect CD spectra, because they have an impact on quartet stacking geometry: CD of G4 structures is primarily determined by the stacking arrangements of guanine base steps within the G-tetrad stacks. Rather counter-intuitively, an all-parallel G4 not always gives a "parallel-type" CD spectra, with a strong positive peak at 260 nm, as the terminal quartet may flip to an all-*syn* conformation. For example, the four 5′-terminal Gs of d[TG^{Me}GGT]$_4$ (^{Me}G = 8-methylguanine) adopt an all-*syn* G-tetrad, altering quartet arrangement and change in CD spectra without changing strand polarity [57]. This again illustrates the fact that CD primarily reflects quartet arrangement, and only indirectly strand orientation.

It is important to emphasize that at first sight, the specific CD spectrum of a parallel G4 is relatively similar to the spectra of an A-form duplex (dsRNA or DNA-RNA duplex). Due to the differences in sugar pucker of a ribonucleotide, most guanosines tend to adopt an *anti* conformation and, as a consequence, the vast majority of RNA G4s are all parallel, with a CD spectrum resembling A-form RNA duplex. Finding a positive peak at 260 nm for an RNA sample is therefore not sufficient to conclude that it is forming a quadruplex, and inaccurate conclusions may possibly be reached based on CD only. On the other hand, differences in ellipticities between potassium or lithium-only conditions may be interpreted as an evidence for G4 formation. Remember, however, that traces of potassium (< 1 mM) may be sufficient to allow RNA G4 formation, and that it may be experimentally difficult to ensure that the buffer is entirely devoid of any "G4-friendly" cation. In any case, significant differences between RNA duplexes and parallel G-quadruplexes may be found at shorter wavelengths (around 200–220 nm). Nevertheless, an alternative method is strongly recommended to confirm G4 formation with an RNA sample [58].

3.3 Nuclear magnetic resonance (NMR)

NMR is a physical phenomenon in which the nuclei of particular isotopes behave as minuscule magnets that precess in a static magnetic field applied externally. The frequency of the precession, also called resonance frequency, is determined by the chemical environment around the nuclei, the isotope, and the strength of the external magnetic field. The resonance frequency of a nucleus of a given isotope in a given static magnetic field is only determined by the chemical surroundings of the nucleus in a molecule or in a complex. As a result, measuring the resonance frequency of the nuclei in a molecule allows us to characterize the molecular chemical environment. NMR has been widely applied in structural studies of small organic molecules and biomacromolecules in solution.

While a complete structural determination is beyond the scope of this section, recording a simple 1D ^{1}H-NMR spectrum *in vitro* is useful to confirm or exclude G4 formation by analyzing the chemical shift of imino protons. When imino protons from guanines or thymines (or uracil for RNA) are involved in hydrogen-bonds or are protected from exchanging with water molecules they become detectable by ^{1}H-NMR. Depending on the type of nucleic acids base-paring these protons will resonate at specific frequencies. For instance, Watson–Crick base pairs CG or AT (as well as AU) usually present one peak around 12–13 ppm [59] and 13–14 ppm [60] respectively. On the other hand, Hoogsteen base pairs such as GG or GU (in RNA) will present two peaks in the 10–12 ppm region [61] (**Figure 5a**).

In the case of G-quadruplex formation, the four imino protons from guanines involved in a G-tetrad will present four peaks in the 10–12 ppm region. As a result, 1D ^{1}H-NMR will easily discriminate between G-tetrads formation and CG or AT base-pairs, but an ambiguity will remain between a G-tetrad and GG or GU base pairs. Depending on the quality of the NMR imino signal, it is also possible to determine the number of Gs implicated in tetrad formation thus we could discriminate two, three or even four layered G4s. Unfortunately, due to the polymorphism of G4 structures, the protons exchange in water solution or the multimerization of G4 structures, the imino signal could be more difficult to interpret. Again, an Li/K comparison could help, as perturbation experiments may be more informative than single measurements. Even so, NMR could at least give information about G4 polymorphism. **Figure 5** shows three examples of G4 where 1D ^{1}H-NMR was a very useful tool to confirm the formation and obtain precise information about their structures. In **Figure 5b**, it is possible to identify in HIVpro1 [62] NMR imino signal eight separate peaks (asterisk symbol) in the range of 10–12 ppm and one isolated peak (triangle) in 13–14 ppm range corresponding to a 2-tetrad G4 with the formation of a GC or AT base pair. NMR also allows to identify other unusual base pairing such as in Ce20 sequence from *C. elegans* [63] (**Figure 5c**; PDB: 7OQT) that presents a non-canonical CT base pair corresponding to the peak (cross) at 10 ppm. Another peak can be assigned to an amino group (-NH_2) buried below the CT base pair and protected from exchanging with water molecules.

Additionally, in a "best case scenario" NMR will be a powerful tool to study G4 ligand interactions, cation coordination sites in G4 structures, detection of intermolecular hydrogen bonds, *etc.* A number of high-resolution NMR structures of inter- and intra-molecular quadruplexes are available in the PDB (https://www.rcsb.org/), and provide invaluable information on G4 structure and dynamics.

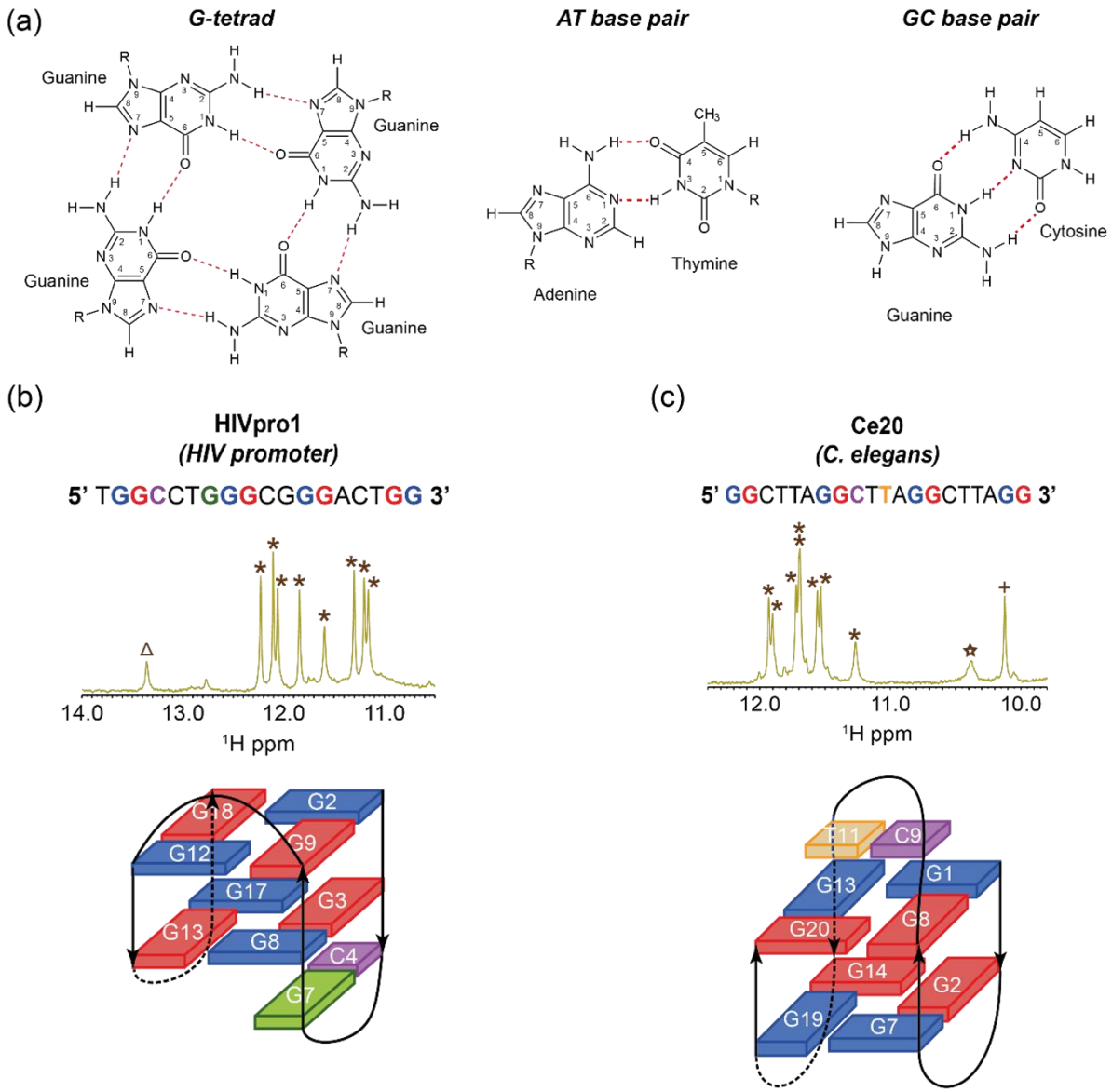

*Figure 5 (**a**) Representation of a G-tetrad based on Hoogsteen-type hydrogen bonds, AT and GC base pairs based on Watson-Crick type hydrogen bonds (hydrogen bonds are in red). 1D ^{1}H-NMR (imino region) with the corresponding sequence and topology from (**b**) HIVpro1 [62] and (**c**) Ce20 in C. elegans genome (PDB: 7OQT) (Adapted with permission from [64]. Copyright 2022, Oxford University Press). Imino protons from G-tetrads are marked with asterisk symbols. Peaks from GC, AT and CT base pairs are respectively marked with triangle, circle and cross symbols. Amino protons have been indicated with a star. NMR experiments have been performed at 20 °C for HIVpro1 and HIVpro3 and 15 °C for Ce20. Sample strand concentrations were between 0.5 mM and 1 mM. Oligonucleotides were dissolved in potassium phosphate buffer 20 mM KPi and 15-70 mM KCl in a volume of 450 µL with 10% D_2O. Spectra were recorded using a double pulse field gradient perfect spin echo (zgesgppe) pulse sequence to suppress the water signal.*

3.4 Molecular size- (or shape-) based characterizations

3.4.1 Gel electrophoresis [65]

A specific migration pattern of a DNA/RNA sample (which must be of high purity – this can be checked first by a denaturing gel) on a native (*i.e.*, non denaturing) gel may provide indication of a secondary structure formation, but rarely gives clues on the nature of the folded form. Gel electrophoresis is a frequently used technique for the identification, quantification, and purification of nucleic acids. The sugar-phosphate backbone of nucleic acids is negatively charged in neutral and alkali environments, allowing the nucleic acid molecules to migrate in an electric field from the negative (cathode) to the positive (anode) pole.

The gel mobility of nucleic acids is determined by their mass, size, shape and charges. Nucleic acids having the same number of nucleotides display a mobility which depends on a number of different parameters, and it is primarily determined by their apparent size and shape (in another words, their structure): large molecules move slowly through the gel while small molecules move faster. In principle, gel electrophoresis should provide information on molecularity. The mobility is expected to decrease as the number of strands involved increases. Intramolecular complexes should migrate faster than bimolecular or tetramolecular ones [66]. However, the situation can be complex, as apparent charges also play a critical role: nucleic acids are polyelectrolytes, around which cations may condense and effectively screen a part of the net charge affecting mobility. Relative mobilities are also affected by acrylamide content and acrylamide/bis-acrylamide ratio. Overall, the mobilities of G4s may differ from those of the corresponding single-strands, and also depend on topology. An accelerated migration may suggest that a particular structure is formed; however, it gives very little information on the nature of the folded form, and any conclusion on molecularity should be taken with precaution.

On the other hand, after performing electrophoresis, a direct way to evidence if some bands correspond to quadruplex species is to post-stain the gel with a G4-specific light-up probe (cf. Part 3.6). One can for example use specific fluorescent G4 ligands such as NMM [67] or ThT [65] (**Figure 6a**) or other light-up probes (*e.g.*, [68]). These dyes provide a straightforward method to identify G4 structures by gel, as these fluorescent probes bind and illuminate exclusively G4 bands. There are two reasons why samples and dyes should not be pre-mixed before gel electrophoresis:

- ***i)*** G4 ligands may actually induce G4 formation in the test tube (*i.e.*, acting as chaperones [69]), leading to altered migration and possible false positives;
- ***ii)*** these ligands may affect the mobility of the sample in the gel. The reference bands are not available if samples and ligands have been mixed before.

Therefore, we recommend to first evidence G4 structures on a gel *via* post-staining first by G4 probe (*e.g.*, NMM may be excited at 393 nm and the emission collected at 610 nm, or ThT with the excitation set at 425 nm and the emission at 490 nm), and then use a "general" staining procedure to evidence all kinds of nucleic acids after washing the gel to remove G4 ligands. SYBR Gold, which is the most widely commercial nucleic acids dye with λ_{ex} at 495 nm and λ_{em} at 537 nm, can stain all types of structures (**Figure 6b**). Compared to G4-specific dyes, this indicator has high affinity for all nucleic acids and cannot be easily removed or replaced by other ligands, explaining why we recommend to use it only after G4 staining.

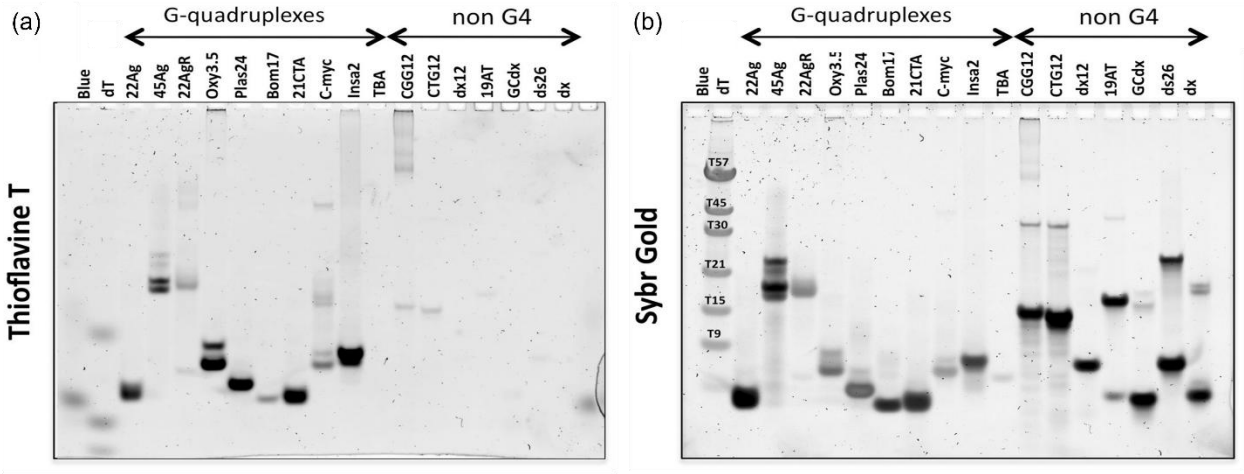

Figure 6 G4 structures shown on 15% native polyacrylamide gel electrophoresis by (a) ThT and (b) Sybr Gold post-staining. Eighteen different oligonucleotides were tested at 2 µM concentration. Samples were prepared in a 50 mM Tris·HCl, pH 7.5, 50 mM KCl. Adapted with permission from [65]. Copyright 2014, Oxford University Press. This gel illustrates one of the limitations of ThT: one quadruplex sample (TBA) is not stained whereas two trinucleotide repeats $(CGG)_{12}$ and $(CTG)_{12}$ are: formation of a G4 with $(CGG)_n$ is a matter of debate, but is clearly not possible for $(CTG)_n$. There are therefore false positives and false negatives; a discussion of the various G4 fluorescent probes follows in the next §.

3.4.2 Size-exclusion HPLC (SE-HPLC)

For a given molecular weight, an oligonucleotide with a higher retention time has a smaller hydrodynamic volume and can therefore be considered as more compact. Hence, SE-HPLC appeared to be a method that could be used to assess the hydrodynamic volume of oligonucleotides in native conditions [70]. One can refer to the work of the Trent and Mergny labs for detailed protocols [70-72]. Compared to gel electrophoresis, SE-HPLC determines the relative proportion of each structure based on absorbance signal. SEC is also compatible with a number of buffer and temperature conditions. It should be noted that SE-HPLC only provides information on the size of a structure, but does not provide direct evidence of G4 folding. Finding appropriate controls is not trivial, and it is hard to find a generic example of 'G4' control,

as quadruplexes have different molecular weights and shapes. We prefer to employ SE-HPLC to study the molecularity of validated structures.

3.4.3 Analytical ultracentrifugation (AUC)

An AUC instrument combines an ultracentrifugation device with an optical readout, typically absorbance, to monitor the behavior of solutes during centrifugation. The solute molecules during the centrifugation process, creating a solvent/solute interface in solution. The shape and the movement speed of this interface are related to the solute weight, density, shape, viscosity, self-polymerization degree and other factors. Therefore, AUC can be used to distinguish G4 structures from other secondary structures [72, 73] and a practical protocol for AUC is available [73]. Despite the relatively specialized instrumentation required for AUC, service centers worldwide provide access, and this method provides a definitive demonstration of folding, and even the information on the shape of the structure.

3.5 Intrinsic fluorescence of nucleic acids

Similarly to isolated nucleosides, single-stranded and double-stranded nucleic acids emit fluorescence upon excitation with UV light; however; due to the emission in the near-UV spectral range (300–400 nm) and low quantum yield (10^{-5} to 10^{-4}) this phenomenon is often considered insignificant. Remarkably, certain secondary structures, in particular G4s, are characterized by a strongly enhanced fluorescence, with broad, red-shifted peaks tailing up to 450 nm and quantum yields reaching ~3×10^{-4}, which is at least 3-fold higher than the corresponding single-strands, although these values depend on the exact sequence and experimental conditions (**Figure 7a & b**) [74]. The fluorescence properties of G4s arise from the formation of excimers in guanine residues defining the core of a G4 structure [75, 76]. Interestingly, some particular G4 motifs, such as G_3T (d[$(G_3T)_3G_3$], PDB: 2LE6) that is prone to dimerization even at low concentrations, as well as left-handed G4s Z-G4 (d[$T(GGT)_4TG(TGG)_3TGTT$], PDB: 2MS9) and Block2 (d[$GT(GGT)_3G$], PDB: 6FQ2) show much stronger fluorescence with quantum yields as high as 3.7×10^{-3} and even more red-shifted emission spectra (λ_{max} = 380–390 nm) [74]. In these cases, the origins of this unusually strong emission arise from the particular '5/6-ring' stacking mode of guanines at the 5′–5′ interface of two G4 units, that gives rise to formation of particularly bright excimers [74, 77, 78]. i-Motif structures also show enhanced fluorescence, although the difference with respect to single-strands and duplexes is more subtle (**Figure 7b**).

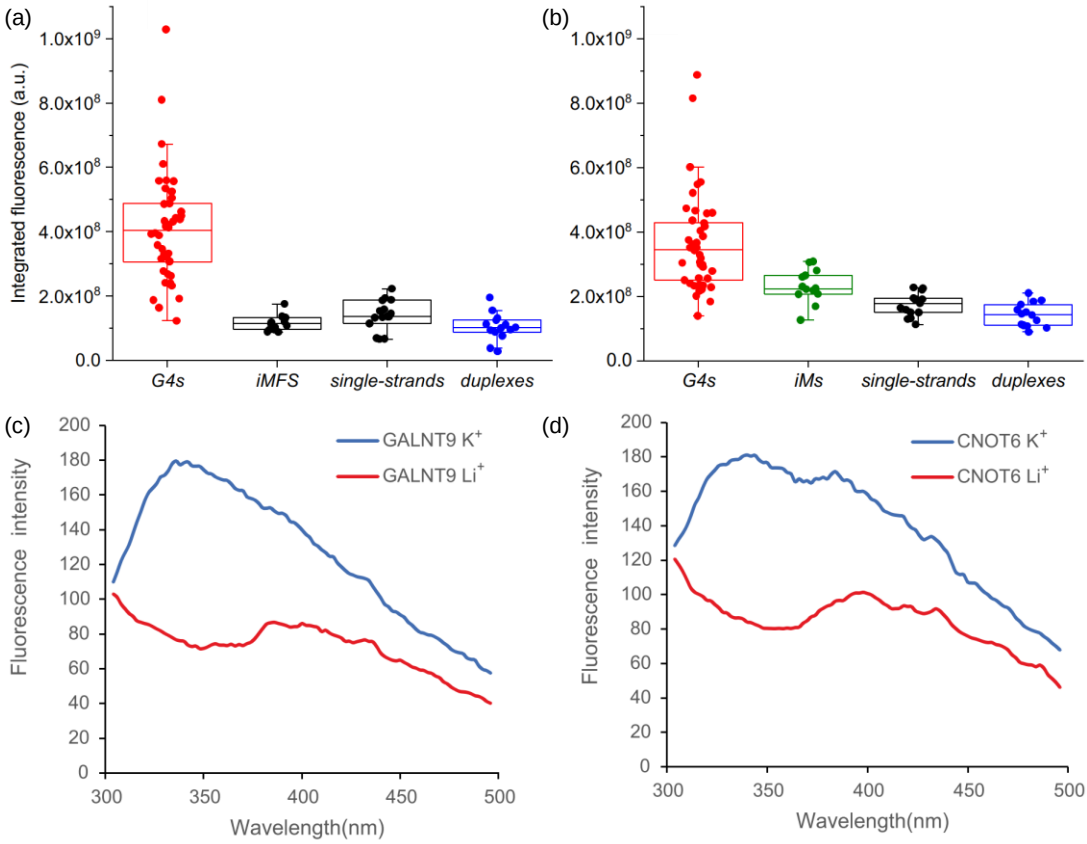

Figure 7 ***(a–b)*** *Box plots of integrated fluorescence intensity of oligonucleotides grouped by their conformations in conditions disfavoring (a) or favoring (b) the formation of i-motifs (iMs) from i-motif-forming sequences (iMFS).* λ_{ex} *= 260 nm,* λ_{em} *= 305 to 505 nm. Adapted with permission from [74]. Copyright 2020, Oxford University Press.* ***(c–d)*** *Intrinsic fluorescence was used to demonstrate the formation of G4 structures in promoter-proximal sequences identified using massively parallel reporter assays: (c) GALN9 (d[*$G_3CTG_5TG_5CAGCCG_4$*]); (d) CNTOT6 (d[*$G_5TAAG_5CG_4CCTG_3$*]). In both cases, fluorescence intensity of 5 µM solutions of oligonucleotides in* K^+ *conditions (150 mM KCl, blue curves) were significantly higher than in* Li^+ *conditions (150 mM LiCl, red curves). Adapted with permission from [79]. Georgakopoulos-Soares et al. copyright 2022 Elsevier Inc.*

In contrast to CD spectra, G4 fluorescence emission spectra are broad and almost unstructured (**Figure 7c & d**), which does not allow one to distinguish between different folding topologies, and an examination of a single fluorescence spectrum of an oligonucleotide is not sufficient to determine the structure. However, a conformational change between unfolded (single-stranded) and folded (G4) structures is easily detectable by fluorescence (**Figure 7c & d**) [74, 80, 81]. Therefore, a comparison of fluorescence spectra of a putative G4-forming sequence in the absence and in the presence of a stabilizing cation (such as K^+) can serve as an additional proof of formation of a G4 structure. This method is gradually gaining popularity in the literature, being employed both in G4-DNA and G4-RNA contexts [79, 82].

Due to low fluorescence quantum yield of nucleic acids, measurement of their intrinsic fluorescence requires a spectrofluorometer with a sufficient signal-to-noise ratio (at least 2000 : 1 in the near-UV range, typically measured using the Raman scatter peak of water). While this performance is readily available with high-quality research instruments, entry-level spectrofluorometers may be inappropriate for using this method [83]. In addition, care must be taken to avoid the traces of fluorescent impurities in water and salts used for the preparation of buffer solutions, as well as in oligonucleotides (that should have at least RP-HPLC purity grade). If these conditions are fulfilled, fluorescence spectra may be recorded with the same samples as used for CD or UV spectroscopy (with a strand concentration of ~5 µM), thereby adding a complementary information with minimal additional costs.

3.6 Fluorescence 'light-up' probes and assays

Fluorescent probes are important tools for G4 characterization *in vitro* and possibly *in vivo*. G4-specific fluorescent dyes with excellent spectroscopic properties are absolutely critical for this assay. The distinct physical properties between single-strands, double-stranded helices and G4 structures offer the possibility of structure-selective binders. Several agents have been reported to bind to the minor groove of B-DNA [84], whereas the most classical mode of interaction between a G4 ligand and a G-quadruplex involves the ligand stacking on the "top" or the "bottom" of the external G-quartets and stabilize G4s in their initial folding topology. A recent report shows that a G4 ligand (PhenDC3) converts a hybrid human telomeric DNA into an anti-parallel chair-type structure and insert into two G-tetrads of the nascent anti-parallel G4 [85]. A G4 ligand can also be sandwiched between two quartets belonging to two different quadruplexes [86]. Flat aromatic molecules interact by π-stacking with the external G-quartets, which is mainly controlled by hydrophobic and *van der Waals* interactions. Ideally, a ligand should have an increased fluorescent quantum yield when bound to G4, acting as a "light-up" probe. Nevertheless, the opposite behavior may be useful for *in vitro* assays.

Regarding *in vitro* applications, the increasing fluorescence emission of a probe in the presence of a G4-forming sequence may be used to evidence G4 formation in a test tube, microtiter plate, or in non-denaturing gels (see Part 3.4). A large number of fluorescent probes that display strong fluorescence enhancement upon G4 binding have been described [87-89]. We therefore introduce representative fluorescent G4 probes (most of them are currently commercially available) from various chemical families. Excitation and emission wavelengths and topologies preferences of G4-specific probes are summarized in Table 2.

i) **Porphyrins**: The electron-deficient system of porphyrins provides strong π-interactions with terminal G-quartets. A very commonly used porphyrin representative is N-methyl mesoporphyrin IX (NMM, **Figure 8a**) [90], which shows high specificity and moderate affinity [91]. NMM has two carboxyl substituents, which are negatively charged at physiological pH and due to electrostatic repulsions cannot engage in interactions with the sugar-phosphate backbone of nucleic acids. Thanks to the electron deficient porphyrin core, the end-stacking binding mode is compatible with NMM-G4 complexes, whereas diagonal and lateral G4 loops hinder stacking, resulting in topological selectivity. Thus, the fluorescence of NMM increases 50–70 fold in the

presence of parallel G4s, ~40-fold in the presence of hybrid structures, and < 20-fold in the presence of anti-parallel G4s, allowing its use as a topological probe of G4 structures [92]. It is still possible for NMM to bind anti-parallel G4s in the 'chair' configuration, which uses lateral loops rather than diagonal loops [93]. TBA, a G4-forming thrombin aptamer, is an appropriate sample to show NMM-'chair' type anti-parallel G4 binding [94]. Note, however, that NMM has a relatively low affinity for TBA, and the same may be true for many other G4 ligands.

ii) **core-substituted Naphthalene Dimide (cNDI)** derivatives: Like porphyrins, naphthalene diimide derivatives (NDIs) have an electron-deficient π-system, exhibiting strong electron affinity and high charge carrier mobility. This electron-accepting core is advantageous for stacking with an electron-rich partner, such as the G-quartet [95]. Additionally, some side chain substituents (like piperazine) adopt hydrogen bonds with the phosphate groups in G4 grooves, further stabilizing the G4-NDI complex [96]. Harnessing the molecule with cationic chains increases affinity towards negative-charged nucleic acids structures, but may have a deleterious effect on conformation selectivity. In fact, the most powerful ligands produce a high and possibly saturated binding response with all nucleic acid structures, regardless of their identity and conformation. Indeed, the *N',N*-dimethylamino moieties of cNDI-1 are protonated at physiological conditions and are responsible of non-specific binding of cNDI-1 to DNA structures [68]. To overcome this problem, Zuffo *et al*. removed the less specific electrostatic interaction between the sugar-phosphate backbone and the protonated amine groups, and topological selectivity emerged at the expense of affinity. cNDI-2 (**Figure 8b**) with terminal hydroxyl groups preferentially binds to parallel G4s, and its fluorescence is enhanced in the presence of parallel G-quadruplexes in the low (8-10) nM range.

iii) **Triphenylmethane (TPM)** derivatives: Various compounds are included in the TPM family, including methyl violet (MV), ethyl violet (EV), methyl green (MEG), malachite green (MG, **Figure 8c**), and crystal violet (CV, **Figure 8d**). These molecules have been shown to have a distinct affinity for intramolecular G4s. Affinities of TPM dyes for an intramolecular G4 (Hum21, $d[G_3(T_2AG_3)_3]$) is inversely correlated to substituent size [97]. High affinity of MG [98] and CV [99] toward Hum21 may be related to the small size of substituents. Similar to porphyrins and cNDIs, MG and CV also interact through end-stacking with the structure. Later on, the end-stacking mechanism of CV-G4 interaction was demonstrated with a stoichiometric ratio of 2:1 (two CV dyes stacked on the two external G-quartets). This stacking mode increases the rigidity of the ligand and subsequently the fluorescence intensity [100]. CV has also been shown to stack on i-motif and enhance fluorescence [101]. CV shows preferential binding to anti-parallel G4s. In contrast to NMM, the loops of an anti-parallel G4 may help define a binding pocket for CV, rather than obstructing its binding. The loop protection is not the only reason that contributes to the increased affinity of CV towards anti-parallel G4s, other factors such as the dimensions of the G4 grooves should also be considered [102].

iv) **Benzothiazole** derivatives: Different from the examples above, benzothiazole derivatives offer a modest flat aromatic surface for stacking. Owing to their positive charges, benzothiazole derivatives become fluorescent upon binding to negatively charged nucleic acids structures due to

restricted intramolecular rotation (RIR) between benzothiazole and dimethylaminobenzene moieties [103]. Thioflavin T (ThT, **Figure 8e**) is a representative example with a fair, but not exquisite, G4 *vs*. duplex discriminating ability. ThT has been used to track G4s in polyacrylamide gels [65]. Similar to NMM, ThT shows relatively low affinity to anti-parallel and hybrid G4s, reducing the accuracy of ThT staining (**Figure 12a**). ThT also has been demonstrated to bind to dsDNA containing "cavity structures" such as an abasic site, a gap site or a mismatch site. The appropriate spaces offered by the cavities and the interaction between ThT and the cavity context bases stabilize the binding [104]. ThT shows the ability to dimerize GA-rich strands in a parallel double-stranded helical structure, accompanied by over 100-fold enhancement in its fluorescence emission [105]. ThT-HE (**Figure 8f**) is a ThT derivative in which the hydroxyethyl was modified on the 3′ nitrogen atom of the thiazole ring. ThT-HE showed preferentially binding to parallel G4s in both potassium and sodium buffers [106].

v) **Styryl** dyes: Preferential fluorimetric response towards G4 structures appears to be a common feature of mono- and distyryl dyes, including long-known mono-styryl dyes used as mitochondrial probes or protein stains. The mono-styryl dyes, DASPMI (**Figure 8g**) or its 4-isomer, are optimal fluorescent light-up probes characterized by high fluorimetric response, excellent selectivity with respect to double-stranded DNA or single-stranded RNA controls, high quantum yield in the presence of G4 analytes (up to 0.32), and large Stokes shift (up to 150 nm). DASPMI preferentially responds to parallel G4s, and the binding of 5 μM dye to 10 μM parallel G4 in 100 mM K^+ buffer can be observed by the naked eye [107]. Distyryl-**1p** (**Figure 8h**) presents complementary binding preference as compared to DASPMI: The fluorescence quantum yield increases up to 550 folds when it binds to anti-parallel G4, and this signal is strong enough to be observed by the naked eye [107].

Fluorescent light-up probes are simpler to use and allow for simultaneous processing of multiple samples; conformation-selective and easy-to-synthesize fluorescent ligands are looked forward in future works. However, it is possible that G4 ligands alter the secondary structure of oligonucleotide strands, as NMM [93] and ThT [103] have both been implicated in DNA conformational rearrangement. In other words, these probes may lead to false positives for G-rich but non-G4 forming strands. The equilibrium of G4 and ligands binding is related to the concentration of each component. Besides a possible switch in topology, high concentrations of ligand may cause aggregation or even precipitation, so we suggest setting ligand concentrations at an equal or lower level than the DNA concentration. Based on our experience, using fluorescent ligands at a concentration of 2 μM with 3 μM of DNAs is sufficient to distinguish between G4 and non-G4s.

Table 2 Summary of G4-specific fluorescently ligands – commercially available and most useful compounds are shown in bold

Families	Abbreviation [CAS No.]	Excitation nm	Emission nm	Binding preference [a]	Ref
Porphyrins	**NMM** [42234-85-3]	380	610	Parallel G4s	[91]
core-extended Naphthalene Diimide derivatives	cNDI-2 (-)	650	687	Parallel G4s	[68]
	cNDI-3 (-)	605	663	Hybrid and anti-parallel G4s	[108]
Triphenylmethane derivatives	**MG** [569-64-2]	617	650	No G4 topology preference	[98]
	CV [548-62-9]	540	650	Anti-parallel G4s	[99]
Benzothiazole derivatives	**ThT** [2390-54-7]	420	490	Possible binding to AG-rich strands and dsDNA cavities	[65]
	ThT-HE [1641591-70-9]	415	485	Parallel G4s	[109]
Styryl derivatives	**DASPMI** [2156-29-8]	450	584	Parallel G4s	[107]
	Distyryl-**1p** [2481650-06-8]	508	570	Anti-parallel G4s	[107]

[a] *Note that this preference is not absolute. For example, NMM shows high affinity to parallel G4s, but can also bind to non-parallel structures (see below).*

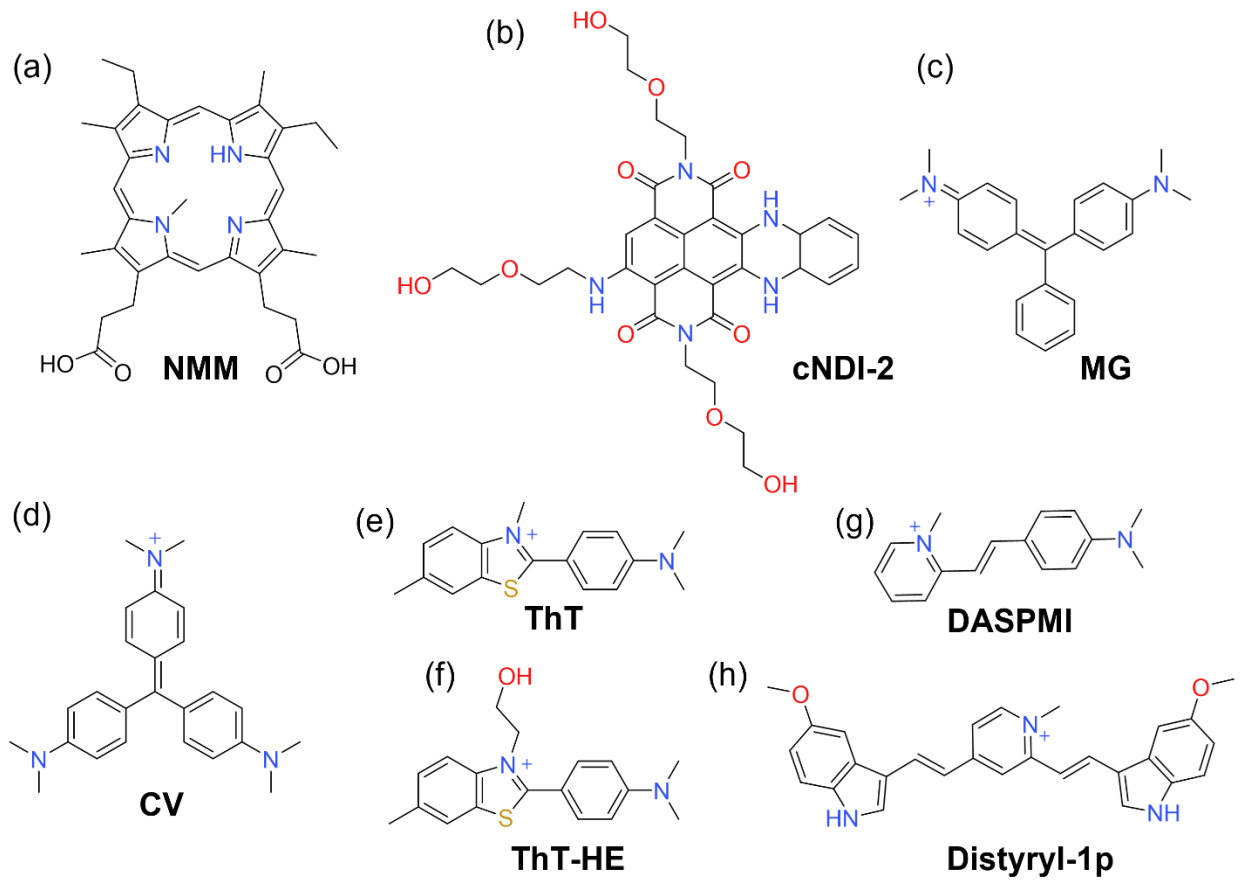

*Figure 8 Chemical structures of (**a**) N-methyl mesoporphyrin IX (NMM), (**b**) cNDI-2, (**c**) Malachite Green (MG), (**d**) Crystal Violet (CV), (**e**) Thioflavin T (ThT), (**f**) ThT-HE, (**g**) DASPMI and (**h**) Distyryl-**1p**.*

Interestingly, a combination of two or more fluorescent probes dramatically improves the discriminatory power of "light-up" assays, allowing one not only to differentiate between G4 and unfolded structures, but also between different topological classes of G4 structures. Thus, a combination of CV and NMM is sufficient to discriminate between parallel G4, anti-parallel G4 and unfolded structures [110] (**Figure 9**). Sensor arrays comprising more than two dyes have an even stronger discriminatory power, allowing to identify hybrid G4 structures as well as duplexes [111]. However, the use of such sensor arrays requires a sufficiently large training set of oligonucleotides with known structures, as well as an implementation of multivariate analysis techniques such as PCA [111] or machine learning [112]. Therefore, such techniques may be more suitable for high-throughput analysis of thousands of oligonucleotides.

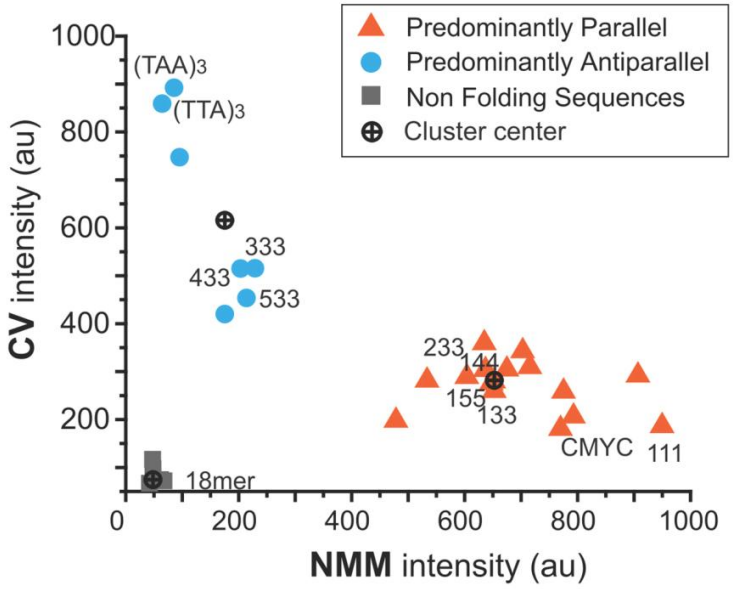

Figure 9 Classification of oligonucleotides into parallel G4, anti-parallel G4, and unfolded groups by using fluorescence output of two dyes (CV and NMM). Adapted with permission from [110]. Copyright 2015, Oxford University Press.

3.7 FRET-based competition assays

Förster Resonance Energy Transfer (FRET) is a known energy transfer mechanism between donor and acceptor chromophores. The energy of a donor chromophore at the electronic excited state is transferred to an acceptor through nonradiative dipole–dipole coupling, resulting in fluorescence quenching of the donor and fluorescence enhancement of the acceptor, unless the latter is 'dark' (*i.e.*, non-fluorescent) [113]. Generally, the FRET efficiency is strongly decreased if the distance between the donor and acceptor is more than 10 nm [114], as the efficiency of energy transfer is inversely related to the sixth power of the distance between the chromophores. Conversely, if the distance between the chromophores is too close, they may form a non-fluorescent intramolecular complex ('contact quenching') [115, 116]. FRET has been employed to study conformational changes (*i.e.*, DNA hybridization [117]) of nucleic acids. Since the folding of intramolecular G4s brings closer the two ends of the oligonucleotide, G4 formation can also be followed by FRET [28]. FRET-melting is a fast method that allows to determine the thermal stability of a G4 [28] or a G4-ligand complex [118]. A rough estimate of T_m is provided by the temperature at which the normalized fluorescence intensity of the donor is 0.5 (**Figure 10**). Compared to UV-melting, FRET-melting can be performed with very fast temperature gradients, as the equilibration within a plastic qPCR plate is much faster than in a quartz cuvette.

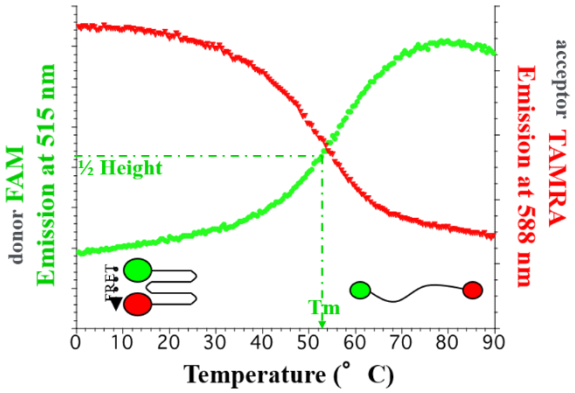

Figure 10 Scheme depicting the validation of G4 structures by FRET melting. Adapted with permission from [28]. Copyright 2001 WILEY- VCH Verlag GmbH, Weinheim, Fed. Rep. of Germany.

With the development of high-throughput sequencing and bioinformatics tools, a vast number of PQS have been predicted, posing challenges for G4 validation *in vitro*. To improve the characterization efficiency and accuracy, we recently developed two FRET-based competition assays, which are based on the competitive binding of a G4 ligand (PhenDC3) between the structure-unknown sequence (competitor) and the G4-forming probe strand, as described in the next two §.

3.7.1 FRET melting competition assay (FRET-MC) [119]

The FRET-MC assay is based on the competitive binding of a G4-selective ligand between a dual-labeled G4 reporter (F21T) and an unlabeled competitor presents in excess. We chose PhenDC3 as the model G4 ligand for FRET-MC assay, taking advantage of its excellent selectivity and affinity towards G4 structures [120]. F21T is a stable G4 structure functionalized at both ends with fluorophores: a 5′-appended donor (FAM) and a 3′-appended acceptor (TAMRA), allowing efficient energy transfer between the donor and acceptor dyes when the oligonucleotide is folded. In principle, any G4-forming sequence competitor would act as a decoy for PhenDC3, meaning that less ligand would be available to stabilize F21T. As a consequence, the T_m value should be close to the one observed in the absence of PhenDC3. On the other hand, if the competitor is not a G4 structure, PhenDC3 remains bound to F21T and increases its T_m (**Figure 11a**). To quantitate this competition effect, we adopted the so-called *S Factor*. In our view, the *S Factor* can be divided into 3 ranges: *i)* $S < 0.3$: G4 competitor; *ii)* $0.3 \leq S < 0.6$: unknown; *iii)* $S \geq 0.6$: non-G4 competitor. To be highlighted, control competitors (well-characterized G4s and non-G4s) are necessary for each FRET-MC experiment (Fluorescent values may vary in function of different instrument, operator, *etc.*: for this reason, it is not possible to compare absolute values with those reported in the literature).

A proper set of control sequences (G4-forming or not) is crucial for these studies. We initially validated this technique with a panel of over 60 sequences, but a smaller set of reference sequences may now be

used. We recommend using the ten sequences listed in Table 3 as controls. RNA counterparts of these sequences may be chosen when dealing with RNA samples.

Table 3 DNA control sequences in FRET-MC

Acronym	Sequence (5′-3′)	Reported conformation	PDB
25TAG	TAGGGTTAGGGTTAGGGTTAGGGTT	hybrid DNA G4	2JSL
23TAG	TAGGGTTAGGGTTAGGGTTAGGG	hybrid DNA G4	2JSK
cmyc	TGAGGGTGGGTAGGGTGGGTAA	parallel DNA G4	1XAV
Pu24T	TGAGGGTGGTGAGGGTGGGGAAGG	parallel DNA G4	2A5P
19wt	GGGGGAGGGGTACAGGGGTACAGGGG	anti-parallel DNA G4	6FTU
c-kit*	GGCGAGGAGGGGCGTGGCCGGC	anti-parallel DNA G4	6GH0
RND4	TAATGAGACTACATTATAAACGTTA	ssDNA	-
dT26	TTTTTTTTTTTTTTTTTTTTTTTTTT	ssDNA	-
ds26	CAATCGGATCGAATTCGATCCGATTG	dsDNA	-
Hairpin 2	TCGGTATTGTGTTTCACAATACCGA	dsDNA	-

Compared to the fluorescence light-up assays, FRET-MC is highly reliable (**Figure 12**) and has been validated by us on many G-rich sequences in the past few years [121-123]. Moreover, FRET-MC is a microvolume (25 μL per sample) assay which can be performed in 96-microwell plates and allows processing dozens of sequences at the same time. All oligonucleotides, except F21T probe, are non-labeled and do not require extensive purification and, in addition, the concentration of each component is fairly low; both these factors are economically beneficial. However, the application of this assay is limited by the heating process; G4 competitors with a low thermal stability are not identified as they appear as single-stranded at the temperature at which F21T unfolds (58.1 °C), leading to false-negative results (**Figure 12c**) [119].

3.7.2 Isothermal FRET competition assay (iso-FRET) [124]

To overcome the limit associated to the poor detection of thermal unstable G4s by FRET-MC, we developed an isothermal FRET competition assay, the so called ‘iso-FRET’ assay. Similar to FRET-MC, iso-FRET is based on the competition between PhenDC3 binding to a G4-forming sequence labelled with a quencher (37Q) and an unknown competitor. A fluorophore-labelled short strand (F22), partially complementary to 37Q, is added to the system to report on the status of 37Q. Depending on the situation, PhenDC3 may either remain bound to 37Q or be drawn towards the competitor present in excess, leading to two possible scenarios (**Figure 11b**):

i) The competitor forms a quadruplex which can bind PhenDC3: As it is 25 times more concentrated than 37Q, there is much less G4 ligand present to bind and maintain the stability of the 37Q quadruplex, leading to duplex formation with F22 and subsequent fluorescence

quenching due to the proximity of the fluorophore (FAM) and quencher (BHQ-1).

ii) Contrarily, when the competitor is not a G4 structure: The high selectivity of PhenDC3 towards G-quadruplexes means that it would bind and stabilize the G-quadruplex formation of 37Q. As a result, F22-37Q hybridization does not take place, and the fluorescence signal of F22 remains unchanged.

Based on the results of a series of competitors, we quantified the competition effect by determining the *F value* at 25 °C and provided our threshold recommendations: *i)* $F < 0.33$: G4 competitor; *ii)* $0.33 \leq F < 0.54$: unknown; *iii)* $F \geq 0.54$: non-G4 competitor.

As iso-FRET is performed in isothermal conditions, it allows to address the issue related to the poor thermally stable, false-negative G4 competitors not identified by FRET-MC, as illustrated in **Figure 12c**. By using the iso-FRET assay, it is theoretically possible to detect G4 competitors characterized by affinities as low as 17 μM toward PhenDC3, which is much higher than all equilibrium dissociation constants (K_d) reported for PhenDC3 towards G4s (in the nM range) [125, 126]. The risk of a false negative in the iso-FRET assay is therefore extremely low. The very same comment applies to FRET-MC: PhenDC3 affinity towards all G4 studied so far is sufficient – by several orders of magnitude – to exclude false negatives.

In addition, the iso-FRET simplifies the data treatment, since it consists in a simple normalization rather than a T_m determination; iso-FRET also increases the throughput from 96 to 384 samples per plate and allows one to characterize G4 structures at physiological temperature.

However, iso-FRET is still not a flawless assay: the competition between 37Q and the competitor partially depends on the affinity for PhenDC3, and, since F22 is a C-rich probe strand, it is possible that a G4-forming competitor hybridizes with F22 and blocks fluorescence quenching, leading to a false-negative result. Therefore, we defined the *CF* factor to describe the complementarity degree between the competitor based on the global base paring alignment:

CF = Numbers of base pairs expected in (F22 - competitor duplex) / Length of F22.

A $CF = 0$ would mean that the competitor is absolutely devoid of any base pairing interaction to F22, while a competitor perfectly complementary to F22 would give the maximal *CF* value of 1. Any DNA competitor with a high level of complementarity to F22 ($CF > 0.86$) should be considered with caution; it may be tested in the absence of PhenDC3 [124]. We recommend adding known negative and positive G4 controls to validate the assay. The competition assay demonstrates a reliable methodology for the high-throughput characterization of G4s.

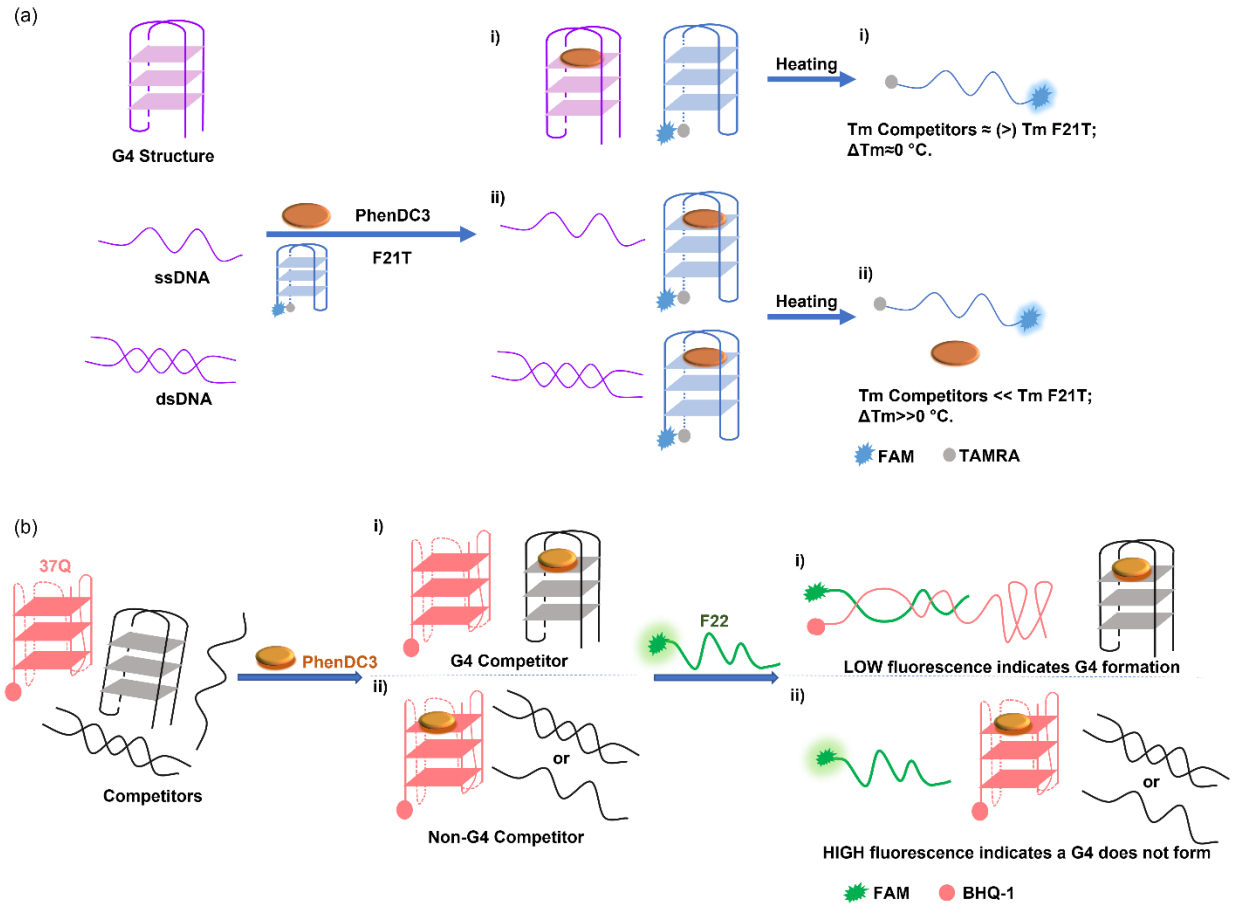

Figure 11 ***(a)*** *Principle of the FRET- MC assay: In the first scenario (top) (i), the competitor forms a quadruplex and traps PhenDC3. In the second scenario (bottom) (ii), the competitor does not form a quadruplex and has no affinity for PhenDC3, which remains bound to F21T (in light blue). Competitor sequences are shown in purple, PhenDC3 is represented as an orange oval, and F21T is represented in blue. Reproduced with permission from [119]. Copyright 2020 Wiley-VCH.* ***(b)*** *Principle of the iso-FRET competition assay: the modified strands (37Q, F22) are shown in color. In the first scenario (top) (i), the competitor (grey) forms a quadruplex and traps PhenDC3 (orange oval), allowing 37Q (red) to quench F22 (green) by forming a duplex. In the second scenario (bottom) (ii), the competitor does not form a quadruplex, PhenDC3 remains bound to 37Q, which cannot hybridize to F22 which emits a strong fluorescence signal. Reproduced with permission from [124]. Copyright 2022, Oxford University Press.*

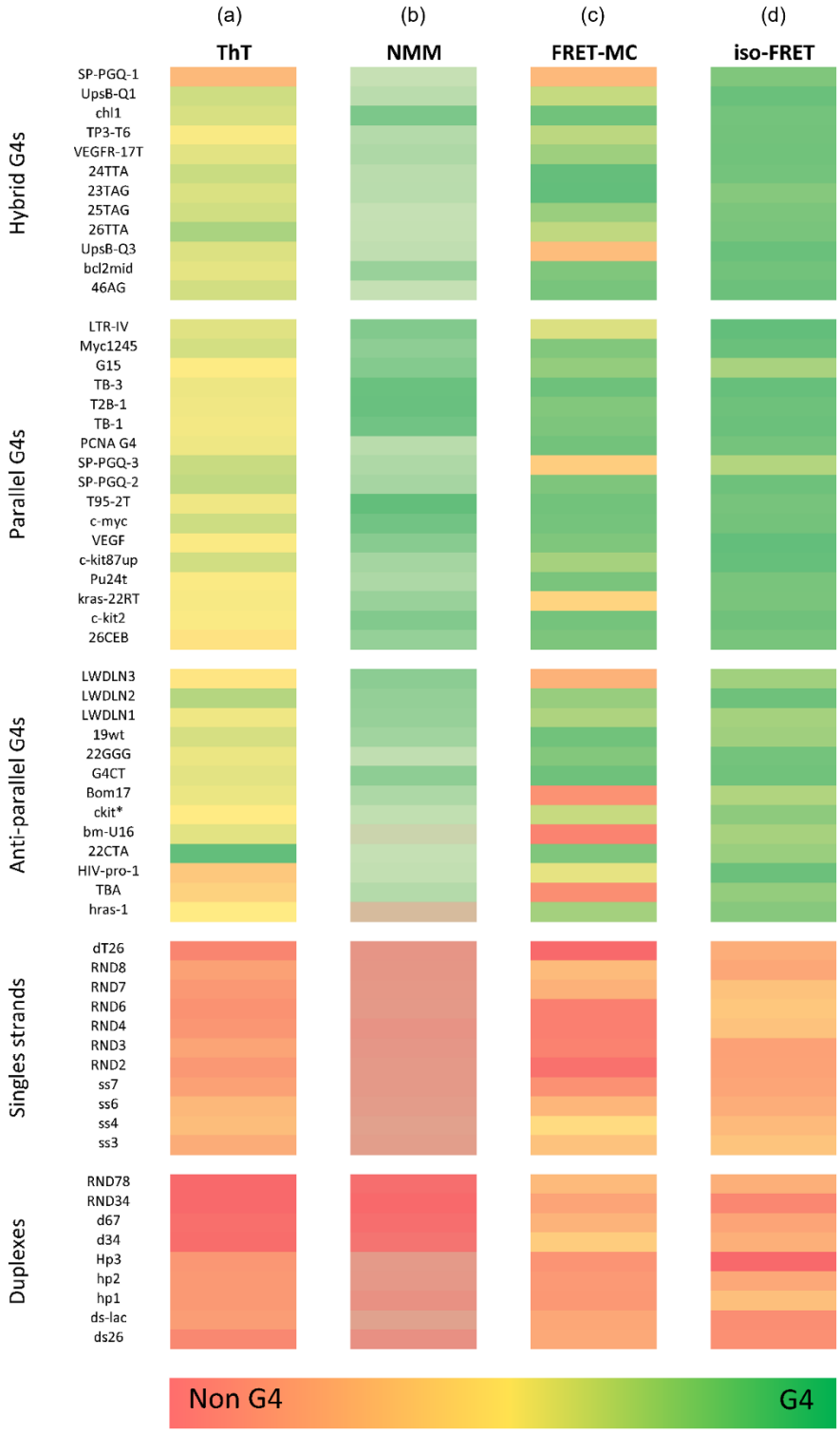

Figure 12 Biophysical characterizations of 61 known sequences. Positive controls (anti-parallel, parallel and hybrid G4) are shown on top, and negative controls (single-strands or duplexes are shown on the lower part of figure. Four different techniques were employed to determine if the sequence adopts a

*quadruplex or not; the conclusion is color-coded from red (non-G4) to green (G4-forming). (**a**) ThT and (**b**)NMM fluorescence staining: 2 µM NMM (or ThT) is incubated with 3 µM pre-folded oligonucleotides for 15 min, samples were measured in 100 mM KCl, 10 mM LiCaco buffer, pH 7.2 at 25 °C; (**c**) FRET-MC results: ΔT_m induced by 0.4 µM PhenDC3 on 0.2 µM F21T, alone or in the presence of 3 µM competitors. Samples were annealed and measured in 10 mM KCl, 90 mM LiCl, 10 mM LiCaco buffer, pH 7.2. Data were extracted from [119]; (**d**) Iso-FRET results: 20 nM F22 is incubated for 24 h in the presence of 200 nM 37Q and 1 µM PhenDC3, alone or in the presence of 5 µM of a variety of competitors. Samples were measured in 20 mM KCl, 80 mM LiCl, 10 mM LiCaco buffer, pH 7.2 at 25 °C. Data were extracted from [124].*

3.8 Additional methods of interest

Additional techniques provide interesting information to characterize these quadruplexes *in vitro*. These methods may not always directly answer the question whether a sequence is forming a G4 or not, but rather provide information on the folded structure. Size exclusion chromatography (SEC) and analytical ultracentrifugation (AUC) allow the analysis of the folding of an unstructured single-strand oligonucleotide into a compact structure upon G4 formation, and we briefly introduced these techniques in §3.4. Mass spectrometry (MS) may also be used to analyze non covalent nucleic acid complexes (for a recent review, [127, 128]). MS offers unique advantages owing to its ability to directly measure strand stoichiometry, even in a mixture. In addition, advanced MS approaches such as reactive probing, fragmentation techniques, ion mobility spectrometry or ion spectroscopy [129] may provide additional information on the complexes.

In addition, even if G4 formation is clear, obtaining reliable information on its stability, molecularity or topology can be difficult in some cases. Some of the methods described here yield information on some, but not all, of these aspects. Determining a high-resolution structure is even more challenging and time-consuming. For instance, guanines involved G-tetrads may be identified using dimethyl sulfate (DMS) footprinting. The N7 position of the guanines involved in Hoogsteen bonding is protected and therefore not methylated by DMS; a subsequent piperidine treatment results in chemical cleavage of the methylated guanine residues. This DMS footprinting experiment involves oligonucleotides labeling and methylation, chemical cleavage, denaturing gel electrophoresis and imaging [130].

4. Summary and perspectives

The seemingly simple question "Is this sequence forming a G-quadruplex *in vitro*?" hides a level of complexity that can be difficult to comprehend. While there are a number of experimental methods available to address this query, however, many of these techniques have limitations that can lead to false positives or false negatives. For this reason, we advocate using a combination of approaches; **Figure 12** illustrates how four different methods can be used to investigate 61 sequences. While not all the assays need to be completed, getting consistent results from two or three independent techniques is recommended to arrive at an unequivocal conclusion. Solid data for a large number of candidate sequences should be advantageous for refining prediction algorithms, particularly for negative controls

(*i.e*., G-rich sequences that fail to adopt a quadruplex structure), or for non-classical G4 in which the impact of special elements (*e.g*., bulges and deficiencies at G-stems, snap-back loops...) is often poorly understood.

The current version of these guidelines is restricted to *in vitro* analyses. A different "Guidelines" paper will be necessary to address how to evidence G4 formation in cells: most of the techniques applicable to biological samples will be different. It will then be interesting to confront G4 formation *in vitro vs.* in cells: while there are hundreds of thousands of candidates G4 sequences in the human genome, not all of them fold into a quadruplex *in vitro*, and this number is probably lower in the cells. Understanding which parameters play a role in this differential behavior is key to understand the biology of G-quadruplexes, but first require reliable approaches to determine actual folding.

Acknowledgments

We thank both reviewers for helpful comments, as well as Patrizia Alberti, Michaela Vorlickova and all our colleagues from the Symbit, ANR Icare and G4Access projects. J.L.M. dedicates this paper to the memory of Prof. Michel Rougée (1933-2022), a precursor in the biophysical analysis of nucleic acids.

Funding

SYMBIT project [CZ.02.1.01/0.0/0.0/15 003/0000477] financed by the ERDF; ANR G4Access [ANR-20-CE12-0023] and ICARE [ANR-21-CE44 to J.L.M.]; Chinese Scholarship Council [201906340018 to Y.L.].

References

1. R.E. Franklin and R.G. Gosling, *Molecular Configuration in Sodium Thymonucleate.* Nature, 1953. **171**(4356): p. 740-741.
2. J.D. Watson and F.H. Crick, *The structure of DNA.* Cold Spring Harb Symp Quant Biol, 1953. **18**: p. 123-31.
3. J.D. Watson and F.H.C. Crick, *Molecular Structure of Nucleic Acids.* Nature, 1953. **171**(4356): p. 737-738.
4. A. Bansal, M. Prasad, K. Roy, and S. Kukreti, *A short GC-rich palindrome of human mannose receptor gene coding region displays a conformational switch.* Biopolymers, 2012. **97**(12): p. 950-962.
5. H. Drew, T. Takano, S. Tanaka, K. Itakura, and R.E. Dickerson, *High-salt d(CpGpCpG), a left-handed Z' DNA double helix.* Nature, 1980. **286**(5773): p. 567-573.
6. P. Khuu, M. Sandor, J. DeYoung, and P.S. Ho, *Phylogenomic analysis of the emergence of GC-rich transcription elements.* Proceedings of the National Academy of Sciences, 2007. **104**(42): p. 16528.
7. J.R. Buzzo, A. Devaraj, E.S. Gloag, J.A. Jurcisek, F. Robledo-Avila, T. Kesler, K. Wilbanks, L. Mashburn-Warren, S. Balu, J. Wickham, L.A. Novotny, P. Stoodley, L.O. Bakaletz, and S.D.

Goodman, *Z-form extracellular DNA is a structural component of the bacterial biofilm matrix.* Cell, 2021. **184**(23): p. 5740-5758 e17.
8. A. Arcella, G. Portella, M.L. Ruiz, R. Eritja, M. Vilaseca, V. Gabelica, and M. Orozco, *Structure of triplex DNA in the gas phase.* J Am Chem Soc, 2012. **134**(15): p. 6596-606.
9. M.D. Frank-Kamenetskii and S.M. Mirkin, *TRIPLEX DNA STRUCTURES.* Annual Review of Biochemistry, 1995. **64**(1): p. 65-95.
10. J.L. Huppert, *Four-stranded nucleic acids: structure, function and targeting of G-quadruplexes.* Chem Soc Rev, 2008. **37**(7): p. 1375-84.
11. J.L. Mergny and D. Sen, *DNA Quadruple Helices in Nanotechnology.* Chem Rev, 2019. **119**(10): p. 6290-6325.
12. C. Chaput John and C. Switzer, *A DNA pentaplex incorporating nucleobase quintets.* Proceedings of the National Academy of Sciences, 1999. **96**(19): p. 10614-10619.
13. J.R. Williamson, M.K. Raghuraman, and T.R. Cech, *Monovalent cation-induced structure of telomeric DNA: the G-quartet model.* Cell, 1989. **59**(5): p. 871-80.
14. N. Maizels and L.T. Gray, *The G4 genome.* PLoS Genet, 2013. **9**(4): p. e1003468.
15. M.J. Law, K.M. Lower, H.P. Voon, J.R. Hughes, D. Garrick, V. Viprakasit, M. Mitson, M. De Gobbi, M. Marra, A. Morris, A. Abbott, S.P. Wilder, S. Taylor, G.M. Santos, J. Cross, H. Ayyub, S. Jones, J. Ragoussis, D. Rhodes, I. Dunham, D.R. Higgs, and R.J. Gibbons, *ATR-X syndrome protein targets tandem repeats and influences allele-specific expression in a size-dependent manner.* Cell, 2010. **143**(3): p. 367-78.
16. A.L. Valton, V. Hassan-Zadeh, I. Lema, N. Boggetto, P. Alberti, C. Saintome, J.F. Riou, and M.N. Prioleau, *G4 motifs affect origin positioning and efficiency in two vertebrate replicators.* EMBO J, 2014. **33**(7): p. 732-46.
17. P. Agarwala, S. Pandey, and S. Maiti, *The tale of RNA G-quadruplex.* Org Biomol Chem, 2015. **13**(20): p. 5570-85.
18. S. Millevoi, H. Moine, and S. Vagner, *G-quadruplexes in RNA biology.* Wiley Interdiscip Rev RNA, 2012. **3**(4): p. 495-507.
19. M. Gellert, M.N. Lipsett, and D.R. Davies, *Helix formation by guanylic acid.* Proc Natl Acad Sci U S A, 1962. **48**(12): p. 2013-8.
20. E. Largy, J.-L. Mergny, and V. Gabelica, *Role of Alkali Metal Ions in G-Quadruplex Nucleic Acid Structure and Stability*, in *The Alkali Metal Ions: Their Role for Life*, A. Sigel, H. Sigel, and R.K.O. Sigel, Editors. 2016, Springer International Publishing: Cham. p. 203-258.
21. F.R. Winnerdy and A.T. Phan, *Chapter Two - Quadruplex structure and diversity*, in *Annual Reports in Medicinal Chemistry*, S. Neidle, Editor. 2020, Academic Press. p. 45-73.
22. N.G. Dolinnaya, A.M. Ogloblina, and M.G. Yakubovskaya, *Structure, Properties, and Biological Relevance of the DNA and RNA G-Quadruplexes: Overview 50 Years after Their Discovery.* Biochemistry (Mosc), 2016. **81**(13): p. 1602-1649.
23. J.L. Mergny, A. De Cian, A. Ghelab, B. Sacca, and L. Lacroix, *Kinetics of tetramolecular quadruplexes.* Nucleic Acids Res, 2005. **33**(1): p. 81-94.

24. B. Sacca, L. Lacroix, and J.L. Mergny, *The effect of chemical modifications on the thermal stability of different G-quadruplex-forming oligonucleotides.* Nucleic Acids Res, 2005. **33**(4): p. 1182-92.
25. M.M. Fay, S.M. Lyons, and P. Ivanov, *RNA G-Quadruplexes in Biology: Principles and Molecular Mechanisms.* J Mol Biol, 2017. **429**(14): p. 2127-2147.
26. M. Mills, P.B. Arimondo, L. Lacroix, T. Garestier, C. Hélène, H. Klump, and J.-L. Mergny, *Energetics of strand-displacement reactions in triple helices: a spectroscopic study11Edited by D. E. Draper.* Journal of Molecular Biology, 1999. **291**(5): p. 1035-1054.
27. L. Lacroix, A. Seosse, and J.L. Mergny, *Fluorescence-based duplex-quadruplex competition test to screen for telomerase RNA quadruplex ligands.* Nucleic Acids Res, 2011. **39**(4): p. e21.
28. J.-L. Mergny and J.-C. Maurizot, *Fluorescence Resonance Energy Transfer as a Probe for G-Quartet Formation by a Telomeric Repeat.* ChemBioChem, 2001. **2**(2): p. 124-132.
29. E. Largy, A. Marchand, S. Amrane, V. Gabelica, and J.L. Mergny, *Quadruplex Turncoats: Cation-Dependent Folding and Stability of Quadruplex-DNA Double Switches.* J Am Chem Soc, 2016. **138**(8): p. 2780-92.
30. M. Nishio, K. Tsukakoshi, and K. Ikebukuro, *G-quadruplex: Flexible conformational changes by cations, pH, crowding and its applications to biosensing.* Biosens Bioelectron, 2021. **178**: p. 113030.
31. D. Miyoshi, A. Nakao, and N. Sugimoto, *Molecular Crowding Regulates the Structural Switch of the DNA G-Quadruplex.* Biochemistry, 2002. **41**(50): p. 15017-15024.
32. M. Cheng, J. Chen, H. Ju, J. Zhou, and J.L. Mergny, *Drivers of i-DNA Formation in a Variety of Environments Revealed by Four-Dimensional UV Melting and Annealing.* J Am Chem Soc, 2021. **143**(20): p. 7792-7807.
33. R. Buscaglia, M.C. Miller, W.L. Dean, R.D. Gray, A.N. Lane, J.O. Trent, and J.B. Chaires, *Polyethylene glycol binding alters human telomere G-quadruplex structure by conformational selection.* Nucleic Acids Res, 2013. **41**(16): p. 7934-46.
34. A. Guedin, J. Gros, P. Alberti, and J.L. Mergny, *How long is too long? Effects of loop size on G-quadruplex stability.* Nucleic Acids Res, 2010. **38**(21): p. 7858-68.
35. S. Amrane, M. Adrian, B. Heddi, A. Serero, A. Nicolas, J.L. Mergny, and A.T. Phan, *Formation of pearl-necklace monomorphic G-quadruplexes in the human CEB25 minisatellite.* J Am Chem Soc, 2012. **134**(13): p. 5807-16.
36. P. Hazel, J. Huppert, S. Balasubramanian, and S. Neidle, *Loop-Length-Dependent Folding of G-Quadruplexes.* Journal of the American Chemical Society, 2004. **126**(50): p. 16405-16415.
37. M. Cheng, Y. Cheng, J. Hao, G. Jia, J. Zhou, J.L. Mergny, and C. Li, *Loop permutation affects the topology and stability of G-quadruplexes.* Nucleic Acids Res, 2018. **46**(18): p. 9264-9275.
38. J. Chen, M. Cheng, G.F. Salgado, P. Stadlbauer, X. Zhang, S. Amrane, A. Guedin, F. He, J. Sponer, H. Ju, J.L. Mergny, and J. Zhou, *The beginning and the end: flanking nucleotides induce a parallel G-quadruplex topology.* Nucleic Acids Res, 2021. **49**(16): p. 9548-9559.
39. S.K. Bharti, J.A. Sommers, J. Zhou, D.L. Kaplan, J.N. Spelbrink, J.L. Mergny, and R.M. Brosh, Jr., *DNA sequences proximal to human mitochondrial DNA deletion breakpoints prevalent in*

human disease form G-quadruplexes, a class of DNA structures inefficiently unwound by the mitochondrial replicative Twinkle helicase. J Biol Chem, 2014. **289**(43): p. 29975-93.

40. V. Brazda, J. Lysek, M. Bartas, and M. Fojta, *Complex Analyses of Short Inverted Repeats in All Sequenced Chloroplast DNAs.* Biomed Res Int, 2018. **2018**: p. 1097018.
41. A. Bedrat, L. Lacroix, and J.L. Mergny, *Re-evaluation of G-quadruplex propensity with G4Hunter*. Nucleic Acids Res, 2016. **44**(4): p. 1746-59.
42. I. Tinoco, *Hypochromism in Polynucleotides1*. Journal of the American Chemical Society, 1960. **82**(18): p. 4785-4790.
43. G.C.K. Roberts, *Encyclopedia of Biophysics*. 2013.
44. P.V. Scaria, S.J. Shire, and R.H. Shafer, *Quadruplex structure of d(G3T4G3) stabilized by K+ or Na+ is an asymmetric hairpin dimer.* Proceedings of the National Academy of Sciences, 1992. **89**(21): p. 10336.
45. J.L. Mergny, J. Li, L. Lacroix, S. Amrane, and J.B. Chaires, *Thermal difference spectra: a specific signature for nucleic acid structures.* Nucleic Acids Res, 2005. **33**(16): p. e138.
46. A. Guedin, L.Y. Lin, S. Armane, L. Lacroix, J.L. Mergny, S. Thore, and L.A. Yatsunyk, *Quadruplexes in 'Dicty': crystal structure of a four-quartet G-quadruplex formed by G-rich motif found in the Dictyostelium discoideum genome.* Nucleic Acids Res, 2018. **46**(10): p. 5297-5307.
47. J.-L. Mergny and L. Lacroix, *Analysis of Thermal Melting Curves.* Oligonucleotides, 2003. **13**(6): p. 515-537.
48. J.L. Mergny and L. Lacroix, *UV Melting of G-Quadruplexes.* Curr Protoc Nucleic Acid Chem, 2009. **Chapter 17**: p. Unit 17 1.
49. Y. Zhang, J. Chen, H. Ju, and J. Zhou, *Thermal denaturation profile: A straightforward signature to characterize parallel G-quadruplexes.* Biochimie, 2019. **157**: p. 22-25.
50. S. Paramasivan, I. Rujan, and P.H. Bolton, *Circular dichroism of quadruplex DNAs: applications to structure, cation effects and ligand binding.* Methods, 2007. **43**(4): p. 324-31.
51. S. Masiero, R. Trotta, S. Pieraccini, S. De Tito, R. Perone, A. Randazzo, and G.P. Spada, *A non-empirical chromophoric interpretation of CD spectra of DNA G-quadruplex structures.* Org Biomol Chem, 2010. **8**(12): p. 2683-92.
52. J.-D. Wen and D.M. Gray, *The Ff Gene 5 Single-Stranded DNA-Binding Protein Binds to the Transiently Folded Form of an Intramolecular G-Quadruplex.* Biochemistry, 2002. **41**(38): p. 11438-11448.
53. D.M. Gray, J.D. Wen, C.W. Gray, R. Repges, C. Repges, G. Raabe, and J. Fleischhauer, *Measured and calculated CD spectra of G-quartets stacked with the same or opposite polarities.* Chirality, 2008. **20**(3-4): p. 431-40.
54. R.C. Monsen, L.W. DeLeeuw, W.L. Dean, R.D. Gray, S. Chakravarthy, J.B. Hopkins, J.B. Chaires, and J.O. Trent, *Long promoter sequences form higher-order G-quadruplexes: an integrative structural biology study of c-Myc, k-Ras and c-Kit promoter sequences.* Nucleic Acids Res, 2022. **50**(7): p. 4127-4147.
55. P. Tothova, P. Krafcikova, and V. Viglasky, *Formation of highly ordered multimers in G-quadruplexes.* Biochemistry, 2014. **53**(45): p. 7013-27.

56. R. Del Villar-Guerra, J.O. Trent, and J.B. Chaires, *G-Quadruplex Secondary Structure Obtained from Circular Dichroism Spectroscopy*. Angew Chem Int Ed Engl, 2018. **57**(24): p. 7171-7175.
57. A. Virgilio, V. Esposito, A. Randazzo, L. Mayol, and A. Galeone, *8-methyl-2'-deoxyguanosine incorporation into parallel DNA quadruplex structures.* Nucleic Acids Res, 2005. **33**(19): p. 6188-95.
58. J. Kypr, I. Kejnovska, D. Renciuk, and M. Vorlickova, *Circular dichroism and conformational polymorphism of DNA.* Nucleic Acids Res, 2009. **37**(6): p. 1713-25.
59. M. Adrian, B. Heddi, and A.T. Phan, *NMR spectroscopy of G-quadruplexes*. Methods, 2012. **57**(1): p. 11-24.
60. S. Dzatko, M. Krafcikova, R. Hansel-Hertsch, T. Fessl, R. Fiala, T. Loja, D. Krafcik, J.L. Mergny, S. Foldynova-Trantirkova, and L. Trantirek, *Evaluation of the Stability of DNA i-Motifs in the Nuclei of Living Mammalian Cells.* Angew Chem Int Ed Engl, 2018. **57**(8): p. 2165-2169.
61. K.D. Berger, S.D. Kennedy, and D.H. Turner, *Nuclear Magnetic Resonance Reveals That GU Base Pairs Flanking Internal Loops Can Adopt Diverse Structures.* Biochemistry, 2019. **58**(8): p. 1094-1108.
62. S. Amrane, A. Kerkour, A. Bedrat, B. Vialet, M.L. Andreola, and J.L. Mergny, *Topology of a DNA G-quadruplex structure formed in the HIV-1 promoter: a potential target for anti-HIV drug development.* J Am Chem Soc, 2014. **136**(14): p. 5249-52.
63. J. Marquevielle, A. De Rache, B. Vialet, E. Morvan, J.L. Mergny, and S. Amrane, *G-quadruplex structure of the C. elegans telomeric repeat: a two tetrads basket type conformation stabilized by a non-canonical C-T base-pair.* Nucleic Acids Res, 2022.
64. J. Marquevielle, A. De Rache, B. Vialet, E. Morvan, J.L. Mergny, and S. Amrane, *G-quadruplex structure of the C. elegans telomeric repeat: a two tetrads basket type conformation stabilized by a non-canonical C-T base-pair.* Nucleic Acids Res, 2022. **50**(12): p. 7134-7146.
65. A. Renaud de la Faverie, A. Guedin, A. Bedrat, L.A. Yatsunyk, and J.L. Mergny, *Thioflavin T as a fluorescence light-up probe for G4 formation.* Nucleic Acids Res, 2014. **42**(8): p. e65.
66. S. Kolesnikova, M. Hubalek, L. Bednarova, J. Cvacka, and E.A. Curtis, *Multimerization rules for G-quadruplexes.* Nucleic Acids Res, 2017. **45**(15): p. 8684-8696.
67. J.S. Smith and F.B. Johnson, *Isolation of G-quadruplex DNA using NMM-sepharose affinity chromatography.* Methods Mol Biol, 2010. **608**: p. 207-21.
68. M. Zuffo, A. Guedin, E.D. Leriche, F. Doria, V. Pirota, V. Gabelica, J.L. Mergny, and M. Freccero, *More is not always better: finding the right trade-off between affinity and selectivity of a G-quadruplex ligand.* Nucleic Acids Res, 2018. **46**(19): p. e115.
69. A. De Cian and J.L. Mergny, *Quadruplex ligands may act as molecular chaperones for tetramolecular quadruplex formation.* Nucleic Acids Res, 2007. **35**(8): p. 2483-93.
70. E. Largy and J.L. Mergny, *Shape matters: size-exclusion HPLC for the study of nucleic acid structural polymorphism.* Nucleic Acids Res, 2014. **42**(19): p. e149.
71. M.C. Miller and J.O. Trent, *Resolution of quadruplex polymorphism by size-exclusion chromatography.* Curr Protoc Nucleic Acid Chem, 2011. **Chapter 17**: p. Unit17 3.

72. M.M. Dailey, M.C. Miller, P.J. Bates, A.N. Lane, and J.O. Trent, *Resolution and characterization of the structural polymorphism of a single quadruplex-forming sequence.* Nucleic Acids Res, 2010. **38**(14): p. 4877-88.
73. W.L. Dean, R.D. Gray, L. DeLeeuw, R.C. Monsen, and J.B. Chaires, *Putting a New Spin of G-Quadruplex Structure and Binding by Analytical Ultracentrifugation.* Methods Mol Biol, 2019. **2035**: p. 87-103.
74. M. Zuffo, A. Gandolfini, B. Heddi, and A. Granzhan, *Harnessing intrinsic fluorescence for typing of secondary structures of DNA.* Nucleic Acids Res, 2020. **48**(11): p. e61.
75. T. Gustavsson and D. Markovitsi, *Fundamentals of the Intrinsic DNA Fluorescence.* Acc Chem Res, 2021. **54**(5): p. 1226-1235.
76. R. Improta, *Quantum mechanical calculations unveil the structure and properties of the absorbing and emitting excited electronic states of guanine quadruplex.* Chemistry, 2014. **20**(26): p. 8106-15.
77. N.T. Dao, R. Haselsberger, M.E. Michel-Beyerle, and A.T. Phan, *Excimer formation by stacking G-quadruplex blocks.* Chemphyschem, 2013. **14**(12): p. 2667-71.
78. C.J. Lech, A.T. Phan, M.-E. Michel-Beyerle, and A.A. Voityuk, *Influence of Base Stacking Geometry on the Nature of Excited States in G-Quadruplexes: A Time-Dependent DFT Study.* The Journal of Physical Chemistry B, 2015. **119**(9): p. 3697-3705.
79. I. Georgakopoulos-Soares, J. Victorino, G.E. Parada, V. Agarwal, J. Zhao, H.Y. Wong, M.I. Umar, O. Elor, A. Muhwezi, J.Y. An, S.J. Sanders, C.K. Kwok, F. Inoue, M. Hemberg, and N. Ahituv, *High-throughput characterization of the role of non-B DNA motifs on promoter function.* Cell Genom, 2022. **2**(4).
80. N.T. Dao, R. Haselsberger, M.E. Michel-Beyerle, and A.T. Phan, *Following G-quadruplex formation by its intrinsic fluorescence.* FEBS Lett, 2011. **585**(24): p. 3969-77.
81. M.A. Mendez and V.A. Szalai, *Fluorescence of unmodified oligonucleotides: A tool to probe G-quadruplex DNA structure.* Biopolymers, 2009. **91**(10): p. 841-50.
82. I. Georgakopoulos-Soares, G.E. Parada, H.Y. Wong, R. Medhi, G. Furlan, R. Munita, E.A. Miska, C.K. Kwok, and M. Hemberg, *Alternative splicing modulation by G-quadruplexes.* Nat Commun, 2022. **13**(1): p. 2404.
83. A.J. Lawaetz and C.A. Stedmon, *Fluorescence Intensity Calibration Using the Raman Scatter Peak of Water.* Applied Spectroscopy, 2009. **63**(8): p. 936-940.
84. S.M. Nelson, L.R. Ferguson, and W.A. Denny, *Non-covalent ligand/DNA interactions: minor groove binding agents.* Mutat Res, 2007. **623**(1-2): p. 24-40.
85. A. Ghosh, M. Trajkovski, M.P. Teulade-Fichou, V. Gabelica, and J. Plavec, *Phen-DC3 Induces Refolding of Human Telomeric DNA into a Chair-Type Antiparallel G-Quadruplex through Ligand Intercalation.* Angew Chem Int Ed Engl, 2022: p. e202207384.
86. A. Funke, B. Karg, J. Dickerhoff, D. Balke, S. Muller, and K. Weisz, *Ligand-Induced Dimerization of a Truncated Parallel MYC G-Quadruplex.* Chembiochem, 2018. **19**(5): p. 505-512.
87. A.C. Bhasikuttan and J. Mohanty, *Targeting G-quadruplex structures with extrinsic fluorogenic dyes: promising fluorescence sensors.* Chem Commun (Camb), 2015. **51**(36): p. 7581-97.

88. E. Largy, A. Granzhan, F. Hamon, D. Verga, and M.-P. Teulade-Fichou, *Visualizing the Quadruplex: From Fluorescent Ligands to Light-Up Probes*, in *Quadruplex Nucleic Acids*, J.B. Chaires and D. Graves, Editors. 2013, Springer Berlin Heidelberg: Berlin, Heidelberg. p. 111-177.
89. X. Xie, B. Choi, E. Largy, R. Guillot, A. Granzhan, and M.P. Teulade-Fichou, *Asymmetric distyrylpyridinium dyes as red-emitting fluorescent probes for quadruplex DNA.* Chemistry, 2013. **19**(4): p. 1214-26.
90. J. Ren and J.B. Chaires, *Sequence and Structural Selectivity of Nucleic Acid Binding Ligands.* Biochemistry, 1999. **38**(49): p. 16067-16075.
91. A. Yett, L.Y. Lin, D. Beseiso, J. Miao, and L.A. Yatsunyk, *N-methyl mesoporphyrin IX as a highly selective light-up probe for G-quadruplex DNA.* J Porphyr Phthalocyanines, 2019. **23**(11n12): p. 1195-1215.
92. N.C. Sabharwal, V. Savikhin, J.R. Turek-Herman, J.M. Nicoludis, V.A. Szalai, and L.A. Yatsunyk, *N-methylmesoporphyrin IX fluorescence as a reporter of strand orientation in guanine quadruplexes.* FEBS J, 2014. **281**(7): p. 1726-37.
93. J.M. Nicoludis, S.P. Barrett, J.L. Mergny, and L.A. Yatsunyk, *Interaction of human telomeric DNA with N-methyl mesoporphyrin IX.* Nucleic Acids Res, 2012. **40**(12): p. 5432-47.
94. R.F. Macaya, P. Schultze, F.W. Smith, J.A. Roe, and J. Feigon, *Thrombin-binding DNA aptamer forms a unimolecular quadruplex structure in solution.* Proceedings of the National Academy of Sciences, 1993. **90**(8): p. 3745-3749.
95. V. Pirota, M. Nadai, F. Doria, and S.N. Richter, *Naphthalene Diimides as Multimodal G-Quadruplex-Selective Ligands.* Molecules, 2019. **24**(3).
96. G.W. Collie, R. Promontorio, S.M. Hampel, M. Micco, S. Neidle, and G.N. Parkinson, *Structural Basis for Telomeric G-Quadruplex Targeting by Naphthalene Diimide Ligands.* Journal of the American Chemical Society, 2012. **134**(5): p. 2723-2731.
97. J.H. Guo, L.N. Zhu, D.M. Kong, and H.X. Shen, *Triphenylmethane dyes as fluorescent probes for G-quadruplex recognition.* Talanta, 2009. **80**(2): p. 607-13.
98. A.C. Bhasikuttan, J. Mohanty, and H. Pal, *Interaction of malachite green with guanine-rich single-stranded DNA: preferential binding to a G-quadruplex.* Angew Chem Int Ed Engl, 2007. **46**(48): p. 9305-7.
99. D.M. Kong, Y.E. Ma, J. Wu, and H.X. Shen, *Discrimination of G-quadruplexes from duplex and single-stranded DNAs with fluorescence and energy-transfer fluorescence spectra of crystal violet.* Chemistry, 2009. **15**(4): p. 901-9.
100. D.-M. Kong, Y.-E. Ma, J.-H. Guo, W. Yang, and H.-X. Shen, *Fluorescent Sensor for Monitoring Structural Changes of G-Quadruplexes and Detection of Potassium Ion.* Analytical Chemistry, 2009. **81**(7): p. 2678-2684.
101. X.Y. Zhang, H.Q. Luo, and N.B. Li, *Crystal violet as an i-motif structure probe for reversible and label-free pH-driven electrochemical switch.* Anal Biochem, 2014. **455**: p. 55-9.
102. D.M. Kong, J.H. Guo, W. Yang, Y.E. Ma, and H.X. Shen, *Crystal violet-G-quadruplex complexes as fluorescent sensors for homogeneous detection of potassium ion.* Biosens Bioelectron, 2009. **25**(1): p. 88-93.

103. V. Gabelica, R. Maeda, T. Fujimoto, H. Yaku, T. Murashima, N. Sugimoto, and D. Miyoshi, *Multiple and Cooperative Binding of Fluorescence Light-up Probe Thioflavin T with Human Telomere DNA G-Quadruplex.* Biochemistry, 2013. **52**(33): p. 5620-5628.
104. L. Liu, Y. Shao, J. Peng, H. Liu, and L. Zhang, *Selective recognition of ds-DNA cavities by a molecular rotor: switched fluorescence of thioflavin T.* Mol Biosyst, 2013. **9**(10): p. 2512-9.
105. S. Liu, P. Peng, H. Wang, L. Shi, and T. Li, *Thioflavin T binds dimeric parallel-stranded GA-containing non-G-quadruplex DNAs: a general approach to lighting up double-stranded scaffolds.* Nucleic Acids Res, 2017. **45**(21): p. 12080-12089.
106. Y. Kataoka, H. Fujita, T. Endoh, N. Sugimoto, and M. Kuwahara, *Effects of Modifying Thioflavin T at the N(3)-Position on Its G4 Binding and Fluorescence Emission.* Molecules, 2020. **25**(21).
107. X. Xie, M. Zuffo, M.P. Teulade-Fichou, and A. Granzhan, *Identification of optimal fluorescent probes for G-quadruplex nucleic acids through systematic exploration of mono- and distyryl dye libraries.* Beilstein J Org Chem, 2019. **15**: p. 1872-1889.
108. M. Zuffo, F. Doria, S. Botti, G. Bergamaschi, and M. Freccero, *G-quadruplex fluorescence sensing by core-extended naphthalene diimides.* Biochim Biophys Acta Gen Subj, 2017. **1861**(5 Pt B): p. 1303-1311.
109. Y. Kataoka, H. Fujita, Y. Kasahara, T. Yoshihara, S. Tobita, and M. Kuwahara, *Minimal Thioflavin T Modifications Improve Visual Discrimination of Guanine-Quadruplex Topologies and Alter Compound-Induced Topological Structures.* Analytical Chemistry, 2014. **86**(24): p. 12078-12084.
110. A. Kreig, J. Calvert, J. Sanoica, E. Cullum, R. Tipanna, and S. Myong, *G-quadruplex formation in double strand DNA probed by NMM and CV fluorescence.* Nucleic Acids Res, 2015. **43**(16): p. 7961-70.
111. M. Zuffo, X. Xie, and A. Granzhan, *Strength in Numbers: Development of a Fluorescence Sensor Array for Secondary Structures of DNA.* Chemistry, 2019. **25**(7): p. 1812-1818.
112. J. Chen, A.D. Gill, B.L. Hickey, Z. Gao, X. Cui, R.J. Hooley, and W. Zhong, *Machine Learning Aids Classification and Discrimination of Noncanonical DNA Folding Motifs by an Arrayed Host:Guest Sensing System.* Journal of the American Chemical Society, 2021. **143**(32): p. 12791-12799.
113. G.A. Jones and D.S. Bradshaw, *Resonance Energy Transfer: From Fundamental Theory to Recent Applications.* Frontiers in Physics, 2019. **7**.
114. C.E. Rowland, J.B. Delehanty, C.L. Dwyer, and I.L. Medintz, *Growing applications for bioassembled Förster resonance energy transfer cascades.* Materials Today, 2017. **20**(3): p. 131-141.
115. M.K. Johansson, H. Fidder, D. Dick, and R.M. Cook, *Intramolecular Dimers: A New Strategy to Fluorescence Quenching in Dual-Labeled Oligonucleotide Probes.* Journal of the American Chemical Society, 2002. **124**(24): p. 6950-6956.
116. S.A.E. Marras, F.R. Kramer, and S. Tyagi, *Efficiencies of fluorescence resonance energy transfer and contact- mediated quenching in oligonucleotide probes.* Nucleic Acids Research, 2002. **30**(21): p. e122-e122.

117. R.A. Cardullo, S. Agrawal, C. Flores, P.C. Zamecnik, and D.E. Wolf, *Detection of nucleic acid hybridization by nonradiative fluorescence resonance energy transfer.* Proceedings of the National Academy of Sciences of the United States of America, 1988. **85**(23): p. 8790-8794.
118. A. De Cian, L. Guittat, M. Kaiser, B. Saccà, S. Amrane, A. Bourdoncle, P. Alberti, M.-P. Teulade-Fichou, L. Lacroix, and J.-L. Mergny, *Fluorescence-based melting assays for studying quadruplex ligands.* Methods, 2007. **42**(2): p. 183-195.
119. Y. Luo, A. Granzhan, D. Verga, and J.-L. Mergny, *FRET-MC: A fluorescence melting competition assay for studying G4 structures in vitro.* Biopolymers, 2021. **112**(4): p. e23415.
120. A. De Cian, E. DeLemos, J.-L. Mergny, M.-P. Teulade-Fichou, and D. Monchaud, *Highly Efficient G-Quadruplex Recognition by Bisquinolinium Compounds.* Journal of the American Chemical Society, 2007. **129**(7): p. 1856-1857.
121. V. Brazda, Y. Luo, M. Bartas, P. Kaura, O. Porubiakova, J. Stastny, P. Pecinka, D. Verga, V. Da Cunha, T.S. Takahashi, P. Forterre, H. Myllykallio, M. Fojta, and J.L. Mergny, *G-Quadruplexes in the Archaea Domain.* Biomolecules, 2020. **10**(9).
122. A. Cantara, Y. Luo, M. Dobrovolna, N. Bohalova, M. Fojta, D. Verga, L. Guittat, A. Cucchiarini, S. Savrimoutou, C. Haberli, J. Guillon, J. Keiser, V. Brazda, and J.L. Mergny, *G-quadruplexes in helminth parasites.* Nucleic Acids Res, 2022. **50**(5): p. 2719-2735.
123. M. Dobrovolná, N. Bohálová, V. Peška, J. Wang, Y. Luo, M. Bartas, A. Volná, J.-L. Mergny, and V. Brázda, *The Newly Sequenced Genome of Pisum sativum Is Replete with Potential G-Quadruplex-Forming Sequences—Implications for Evolution and Biological Regulation.* International Journal of Molecular Sciences, 2022. **23**(15).
124. Y. Luo, D. Verga, and J.L. Mergny, *Iso-FRET: an isothermal competition assay to analyze quadruplex formation in vitro.* Nucleic Acids Res, 2022. **50**: p. e93.
125. L. Bonnat, L. Bar, B. Gennaro, H. Bonnet, O. Jarjayes, F. Thomas, J. Dejeu, E. Defrancq, and T. Lavergne, *Template-Mediated Stabilization of a DNA G-Quadruplex formed in the HIV-1 Promoter and Comparative Binding Studies.* Chemistry, 2017. **23**(23): p. 5602-5613.
126. L. Bonnat, M. Dautriche, T. Saidi, J. Revol-Cavalier, J. Dejeu, E. Defrancq, and T. Lavergne, *Scaffold stabilization of a G-triplex and study of its interactions with G-quadruplex targeting ligands.* Org Biomol Chem, 2019. **17**(38): p. 8726-8736.
127. V. Gabelica, *Native Mass Spectrometry and Nucleic Acid G-Quadruplex Biophysics: Advancing Hand in Hand.* Accounts of Chemical Research, 2021. **54**(19): p. 3691-3699.
128. E. Largy, A. König, A. Ghosh, D. Ghosh, S. Benabou, F. Rosu, and V. Gabelica, *Mass Spectrometry of Nucleic Acid Noncovalent Complexes.* Chemical Reviews, 2022. **122**(8): p. 7720-7839.
129. S. Daly, F. Rosu, and V. Gabelica, *Mass-resolved electronic circular dichroism ion spectroscopy.* Science, 2020. **368**(6498): p. 1465-1468.
130. D. Sun and L.H. Hurley, *Biochemical techniques for the characterization of G-quadruplex structures: EMSA, DMS footprinting, and DNA polymerase stop assay.* Methods Mol Biol, 2010. **608**: p. 65-79.